PHILOSOPHICAL TRANSACTIONS OF THE ROYAL SOCIETY A

rsta.royalsocietypublishing.org

Review

Cite this article: Gu X, Gunkel I, Russell TP. 2013 Pattern transfer using block copolymers. Phil Trans R Soc A 371: 20120306. http://dx.doi.org/10.1098/rsta.2012.0306

One contribution of 17 to a Theme Issue 'Molecular nanostructure and nanotechnology'.

Subject Areas:
nanotechnology, chemical physics

Keywords:
block copolymer, self-assembly, pattern transfer, lithography, nanotechnology

Author for correspondence:
Thomas P. Russell
e-mail: russell@mail.pse.umass.edu

Pattern transfer using block copolymers

Xiaodan Gu[1], Ilja Gunkel[1,2] and Thomas P. Russell[1]

[1]Polymer Science and Engineering Department, University of Massachusetts at Amherst, 120 Governors Drive, Amherst, MA 01003, USA

[2]Advanced Light Source, Lawrence Berkeley National Laboratory, 1 Cyclotron Road, Berkeley, CA 94720, USA

To meet the increasing demand for patterning smaller feature sizes, a lithography technique is required with the ability to pattern sub-20 nm features. While top-down photolithography is approaching its limit in the continued drive to meet Moore's law, the use of directed self-assembly (DSA) of block copolymers (BCPs) offers a promising route to meet this challenge in achieving nanometre feature sizes. Recent developments in BCP lithography and in the DSA of BCPs are reviewed. While tremendous advances have been made in this field, there are still hurdles that need to be overcome to realize the full potential of BCPs and their actual use.

1. Introduction

Current developments in the semiconductor industry are focused on the minimization of device size using various improved lithographic techniques. One of the key challenges is to fabricate smaller device dimensions to meet Moore's law [1]. Photolithography, even with state-of-the-art 193 nm immersion technology with multiple-patterning ability, is extremely hard to scale below 22 nm. An alternative approach to the standard 'top-down' photolithographic approaches is a 'bottom-up' approach based on self-assembly. The self-assembly of block copolymers (BCPs) has attracted significant attention owing to the small feature sizes that can be obtained, the highly parallel nature of the process and the ease of chemically modifying the BCP or selectively removing one of the components. Currently, feature sizes down to 3 nm can be achieved from the self-assembly of BCPs and, possibly, even smaller feature sizes can be achieved [2]. There is no question that sub-nanometre feature sizes can be obtained by

combining the self-assembly of BCPs with naturally occurring biomolecules, such as cyclic peptides [3]. Exciting progress has been made in the past decades using the self-assembly of BCPs on many fronts, including the feature sizes, line-edge roughness, lateral ordering and etch contrast. In concert with 'top-down' approaches, the guided self-assembly, commonly referred to as directed self-assembly (DSA), of BCPs offers a potential strategy for device fabrication to maintain Moore's law for a longer period of time, yielding devices with areal densities in excess of 10 teradots per inch^2. There are, nevertheless, still challenges that must be met to achieve this goal.

To take full advantage of the nanostructures offered by the DSA of BCPs, highly selective pattern-transfer techniques with high fidelity are required. Typically, two steps are needed to transfer the BCP pattern. Since BCPs consist of two organic polymer chains covalently linked together at one end, there is little natural etching contrast between the blocks. To overcome this, a variety of techniques, depending on the nature of the BCP, have been developed to selectively remove one of the blocks, leaving behind a polymer film with pores or isolated nanoscopic features that can function as an etching mask for further pattern transfer. Even with this contrast, the fidelity of the transfer must be high to ensure precise pattern transfer. Different pattern-transfer techniques, including dry etching, wet etching and ion beam etching, have been used for pattern transfer of BCP templates to other materials.

This review article focuses on the generation of masks from BCPs and their use for pattern transfer. We focus on describing different methods for producing masks from the self-assembly of BCPs. The reader is referred to several general reviews describing the phase behaviour and ordering of BCPs in thin films and related topics [4–11]. In this review, we will provide a general introduction to BCP lithography and pattern-transfer techniques, then a summary of the lithographic masks generated from different types of BCPs and examples of transfer, then a brief description of DSA processes, and, finally, challenges and possible future research directions involving BCP lithography and pattern-transfer processes.

(a) Block copolymer self-assembly

BCPs consist of two chemically distinct polymers that are covalently linked at one end. Non-favourable segmental interactions, coupled with the inherent entropic loss due to the long-chain nature of the BCP, cause a separation of the blocks into domains where the size of the domains is dictated by the molecular weight of the BCP chain and the shape of the domain, be it spherical, cylindrical, gyroid or lamellar, is dictated, primarily, by the volume fraction of the components. Since the polymer chains are covalently bonded together, the size scale of the domains must be commensurate with the size of the polymer chain, typically on the tens of nanometres length scale or less. The domains that are formed are typically referred to as microdomains (even though they are nanoscopic in size) where, at the time of the initial theoretical developments in the field by Meier [12] and Helfand & Wasserman [13], microscopic was considered to be very small. The lower limit of the microdomain size is set by the condition (for symmetric BCPs, i.e. where the volume fractions of the components are equal) that $\chi N > 10.5$ [14], where χ is the Flory–Huggins segmental interaction parameter and N is the total number of units constituting the BCP, i.e. the degree of polymerization (DP). If $\chi N < 10.5$, then the blocks of the BCP will mix, forming a homogeneous or phase-mixed morphology. So, to decrease the size and maintain a microphase-separated morphology, N must decrease and χ must increase to compensate.

The morphology of BCP thin films depends on the strength of interfacial interactions. Strong preferential interactions of one block with the substrate or a lower surface energy of one component cause a segregation of that block to either the surface of the film or the substrate interface. The connectivity of the blocks forces a parallel orientation of the microdomains to the substrate. When the surface is neutral, i.e. the interfacial interactions are balanced (equally favourable or unfavourable), there is no preferential segregation of the components to the interfaces. Any slight incommensurability will cause the microdomains to orient normal to the

surface. The interfacial energies of a BCP can be precisely controlled by anchoring a random copolymer to the surface, where the volume fraction, f, of monomers in the brush can be varied in the synthesis. As f is varied from 0 to 1, the system goes from a condition of preferential wetting of the substrate by A to a preferential wetting by B. However, for one value of f the interactions of A and B with the substrate are balanced. At this point, the microdomains of the BCP will orient normal to the surface. This simple concept of balancing interfacial interactions, whether this is done with an anchored random copolymer, a cross-linked random copolymer material or even, as shown recently, a partial coverage of a BCP on the substrate or by passivating a surface, so as to control the orientation of the BCP microdomains, has had a profound impact on the use of BCPs as templates for pattern transfer or as scaffolds for the fabrication of nanostructured materials.

(b) Pattern-transfer methods

(i) Dry etch

Dry etch is widely used for the transfer of a resist mask pattern to an underlying material in the semiconductor industry. Dry etch is typically used for directional etching, since the etchant gas is ionized by a high-radio-frequency (RF) field and ions are accelerated towards the surface by an electric field. The highly energetic ions can chemically react with the etch mask and the underlying substrate, and physically remove material by a sputtering mechanism. Provided the pitch of the features is approximately greater than 22 nm, the mask determines the lateral resolution of the transferred pattern. However, the achievable depth of the etch profile is limited by the thickness of the mask material, the selectivity of the etchant and the fidelity of the etch. While, in principle, the etching is unidirectional, the divergence of the beam and scattering events in the medium can cause a spreading of the etching, and material removed from underneath the mask, i.e. there is an undercut, will limit both the lateral resolution of the etching and the aspect ratio of the features produced. In addition, for BCP templates, as the size scale of the features is reduced, usually the thickness of the template is reduced, which can limit the fidelity of the transfer; if there is not a large selectivity in the etching rates, the fidelity of the transfer can be compromised. Reactive ion etching (RIE) with oxygen will effectively oxidize and remove most organic polymers. For silicon (Si) and metals, fluorine-based etch chemistry, using fluorinated gases, such as SF_6, C_2F_8 or CHF_3, in combination with argon (Ar) gas, are most effective. The etch rates depend on the different ionization and acceleration conditions. Typically, a higher RF power increases the ion density, and, consequently, the etch rate. Ion milling, typically using Ar ions, is similar to RIE, but based on a directional sputtering process.

(ii) Wet etch

The principle of wet etch is similar to dry etching, but the etchant is delivered to the surface in a liquid medium, as opposed to being a stream of accelerated ions. Wet etching for most amorphous or disordered crystalline materials is isotropic, since there is no directional biasing of the chemical reactions at the interface. However, if the substrate is a single crystalline material, such as a silicon wafer, then certain etchants will preferentially etch along certain lattice planes. For example, with Si, using a potassium hydroxide (KOH) solution, the etch rate of Si along the (111) plane is much slower than along the (110) plane. This difference in etching rates can be used to produce trigonal, saw-tooth or pyramidal-type facets on the surface with exceptional fidelity along the lattice planes [15,16].

A directional wet etch can also be achieved using a metal-assisted chemical etch process. Here, noble metals, along with hydrogen peroxide (H_2O_2) and hydrogen fluoride (HF), are used for local oxidation and reduction reactions, which will etch Si. Metals, such as gold, deposited on the surface of Si serve as a local cathode to catalyse the reduction of H_2O_2 and to oxidize silicon to form SiO_2, which can subsequently be removed by HF. This process results in the removal of Si

without a net consumption of the metal. Therefore, the metal etches into Si, and acts as a negative resist etch mask. Under controlled etching conditions, a metal-assisted chemical etch produces ultra-high-aspect-ratio silicon structures.

2. Block copolymer lithography: organic block copolymer templates

The application of BCPs for nanoscale lithography has been an active research area. Here, we review BCP lithography based on the chemical structure of the different BCPs that are typically used. We will further discuss different ways for pattern transfer using those BCPs. Different methods, which are aimed to enhance the etching contrast of the organic BCP, will be discussed along with the corresponding pattern-transfer methods.

(a) PS-*b*-PI and PS-*b*-PB

The idea of using BCPs for lithography patterning was first introduced by Mansky *et al.* [17,18]. After the observation of well-ordered hexagonally packed spherical domains in a thin film by transmission electron microscopy (TEM), they realized that BCP microdomains could potentially be used for high-resolution lithography. Later, the first experimental work on BCP lithography was demonstrated by Park *et al.* [19] using thin films of sphere-forming poly(styrene-*b*-butadiene) (PS-*b*-PB) and poly(styrene-*b*-isoprene) (PS-*b*-PI) BCPs. In this experiment, thin films of the BCPs were spin-coated onto a silicon wafer and, then, thermally annealed to allow the BCPs to self-assemble into a periodic array of PB spherical microdomains embedded in a PS matrix. By ozone removal or staining of the PB block with osmium tetroxide (OsO_4), a template with sufficient contrast for patterning using O_2 RIE was produced. A periodic array of holes or pillars (aspect ratio approx. 1; area density approx. 0.1 teradot cm^{-2}) was patterned into a Si_3N_4 substrate by CF_4/O_2 RIE, which was comparable to the areal densities afforded by the state-of-the-art e-beam lithography at that time (figure 1). This first example demonstrates the beauty in the use of self-assembly of BCPs to generate a pattern for transfer. First, the self-assembly is highly parallel, occurring uniformly over large areas simultaneously. Second, high areal densities can be achieved relatively simply without the need of multi-step, photolithographic processes.

The pattern transfer of BCP morphologies was further extended to other materials, such as Ge substrates [20]. Also, selective deposition of GaAs pillars on the porous structure was demonstrated by using a PS-*b*-PI BCP template [21]. Although progress has been made, one of the disadvantages of the above-described method is that the sphere-forming PS-*b*-PB BCP was not useful for the patterning of a high-aspect-ratio structure because of the limited thickness of masks that are fabricated from sphere-forming microdomains. A rather complicated three-layer structure, including a PS-*b*-PI BCP layer, a Si_3N_4 intermediate layer and a polyimide polymer layer, was used to circumvent the problem mentioned above, enabling the patterning of high-aspect-ratio structures [22]. The Si_3N_4 intermediate layer was chosen to take advantage of the high selectivity between the hard Si_3N_4 mask and the underlying polyimide layer during O_2 RIE. Therefore, after the transfer of the spherical microdomain structure to Si_3N_4, subsequent etching through the Si_3N_4 to the underlying polyimide layer produced a high-aspect-ratio polyimide structure. However, this trilayer pattern-transfer strategy is rather tedious and its applicability is limited when compared with other BCPs, such as polystyrene-*block*-poly(methyl methacrylate) (PS-*b*-PMMA). After this pioneering work, the number of publications in the field of BCP lithography and the number of laboratories focused on this topic have exploded.

(i) PS-*b*-PMMA

PS-*b*-PMMA is the most widely studied BCP system because of its wide commercial availability, narrow molecular weight distributions of each block and PMMA being a standard photoresist. Moreover, the surface energies of PS and PMMA are very similar, and convenient control over the

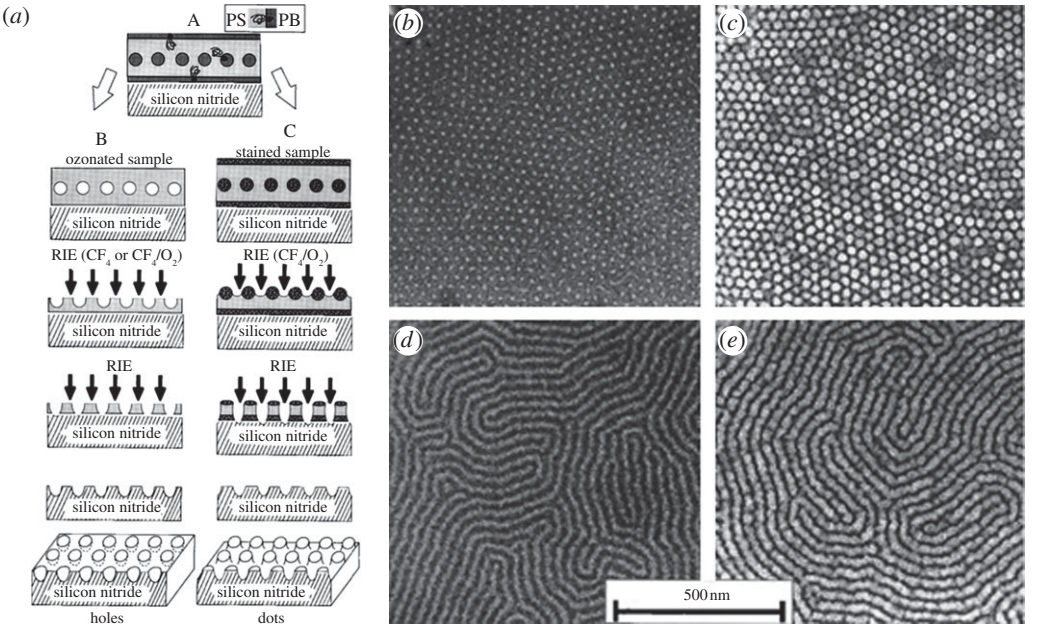

Figure 1. (*a*) Schematic of the pattern-transfer process from PS-*b*-PB to a silicon nitride substrate. (*b*) Spherical microdomain monolayer film before RIE. The lighter regions are the PB domains that were degraded and removed by ozonation, and the darker background is the PS matrix. (*c*) Hexagonally ordered array of holes in silicon nitride after RIE. The pattern was transferred from a copolymer film such as that in (*b*). The lighter regions are 15 nm deep holes that were etched out. (*d*) A cylindrical microdomain monolayer film before RIE. The darker lines are osmium-stained PB cylinders that lie parallel to the surface. (*e*) Fingerprint-like lines in silicon nitride after RIE. The pattern was transferred from a copolymer film such as that in (*d*). The darker regions are 15-nm-thick ridges in the silicon nitride, which were protected from RIE. (Reproduced with permission from [19]. Copyright © 1997 AAAS.)

domain orientation can be achieved by tuning the interfacial energy of the underlying substrate with a random copolymer brush, by applying an external field, such as an electric field, or by use of solvent evaporation, a highly directional field normal to the film surface [23,24]. The easy removal of PMMA and the cross-linking of PS, using standard, non-disruptive processes, has made the BCP a very attractive candidate for lithography and subsequent applications.

Russell and co-workers first fabricated porous polymer templates using PS-*b*-PMMA either by destructive UV radiation of the sample or by reversible, selective solvent reconstruction of thin films. Thurn-Albrecht *et al.* [25] first reported a simple route to fabricate a porous polymer template using a PS-*b*-PMMA BCP by selectively degrading the PMMA block using UV light. Thin films of PS-*b*-PMMA were spin-coated onto a silicon substrate where interfacial interactions were balanced using a random copolymer (PS-*r*-PMMA) anchored to the surface of random brush copolymers in order to promote an orientation of the cylindrical PMMA microdomains normal to the surface. By thermal annealing, an array of cylindrical microdomains of PMMA in a PS matrix, oriented normal to the film surface, was obtained over the entire surface. Exposure of the film to UV radiation degraded the PMMA, cross-linked the PS and, upon rinsing with dilute acetic acid, led to a stable, nanoporous film in direct contact with the substrate, where the nanopores ran from the surface to the substrate and the pore diameter was equal to that of the original cylindrical microdomains [25]. Figure 2 shows a scanning electron microscopy (SEM) image of the porous polymer template. Both X-ray and neutron scattering were used to demonstrate the porous structure, where the increase in the scattered intensity could be quantitatively accounted for by the change in the electron density or neutron scattering length density of the template, before and after removal of the PMMA block.

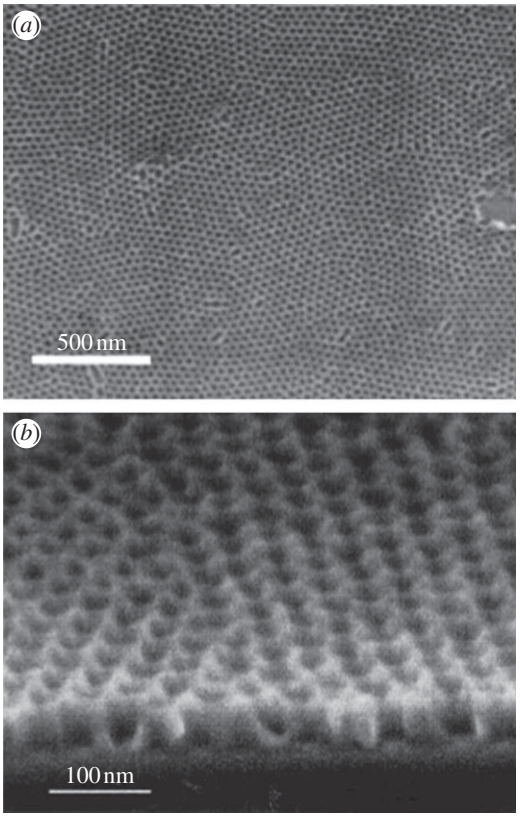

Figure 2. (*a*) SEM top view and (*b*) side view of a porous PS template after removing the PMMA blocks from a PS-*b*-PMMA BCP thin film. (Reproduced with permission from [25]. Copyright © 2000 John Wiley & Sons, Inc.)

Surface reconstruction, first introduced by Xu *et al.* [26,27], affords another convenient method to generate a porous BCP template. PS-*b*-PMMA thin films, where the cylindrical microdomains were oriented normal to the film surface and the thickness of the BCP was approximately one period, were immersed in a good solvent for the PMMA block but a non-solvent for the PS matrix. The strong solvating power of the solvent draws the PMMA block (still covalently bound to the PS block) to the surface and, upon drying, the PMMA chains are deposited on the surface, leaving pores in the place where the cylindrical microdomains were. X-ray photoelectron microscopy experiments showed that the PMMA completely covered the surface. This trivial reconstruction process leaves a porous template in direct contact with the substrate and, unlike the process where the PMMA is degraded, if the reconstructed film is heated above the glass transition temperature of the two blocks ($T_{g,PS} = 100^{\circ}C$ and $T_{g,PMMA} = 115^{\circ}C$), then the PMMA is drawn back into the pores, leaving the original films. This return to the original film by drawing the PMMA back into the pores can be used to generate an entirely new array of templates, as shown by Park *et al.* [28].

The centre-to-centre distance and the pore diameter in porous PS-*b*-PMMA templates can be controlled in several ways. One approach is to vary the molecular weight of the BCP. Here, both the period and the diameter of the cylindrical microdomain will be varied together. In another approach, PMMA homopolymer can be added to the BCP to increase the diameter of the cylindrical microdomain, while only increasing the centre-to-centre distance by an amount that is commensurate with the increase in the diameter of the microdomain. Here, by selectively decomposing the PMMA block or by use of a selective solvent, a pore diameter commensurate with the cylindrical microdomain will be obtained [29]. However, if the reconstructed film is thermally annealed, then the PMMA covalently bound to the PS block will be drawn back into

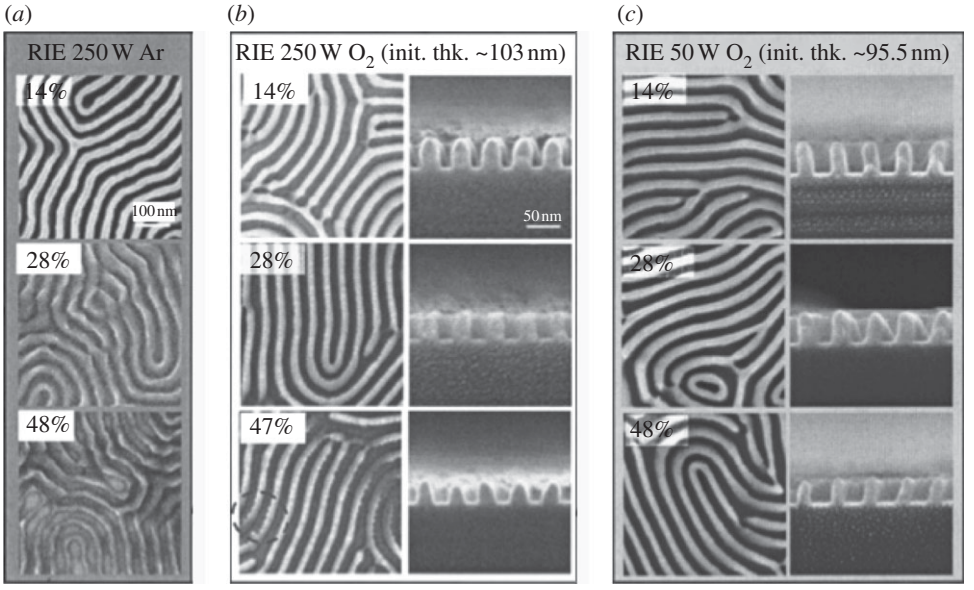

Figure 3. Top-down and cross-sectional SEM images of a polymer mask formed by different etching of PS-*b*-PMMA. (*a*) A PS-*b*-PMMA BCP etched in Ar RIE. (*b*) A PS-*b*-PMMA BCP etched in O_2 RIE with high power (250 W). (*c*) A PS-*b*-PMMA BCP etched in O_2 RIE with low power (50 W). (Reproduced with permission from [32]. Copyright © 2007 AVS Science and Technology of Materials, Interfaces, and Processing.)

the pores, while the homopolymer would have been completely solubilized and removed. The depletion of the PMMA can result in a depression in the height of the film at the location of the cylindrical microdomains or, as shown by Jeong *et al.* [29], a smaller pore can be produced running down the core of the cylindrical microdomain. Consequently, the period can be kept fixed and a smaller pore diameter can be achieved [29]. In a third approach, cross-linking the PS matrix in PS-*b*-PMMA BCPs by ozone plasma has also been demonstrated to generate pores with relatively small size [30]. The size of the pores ranged from 3 to 8 nm [31]. The pores were opened at the centre of the PMMA domains as the polymer chains relax when the thin film contracts during the cross-linking.

One of the fundamental limitations in processes requiring the use of a fluid to remove one of the components or degradation by-products is the capillary force. In particular, if the aspect ratios of features that are tens of nanometres in size are too large, then, as the fluid is removed, capillary force will pull adjacent features towards each other, causing a collapse of the structure [32]. There are several routes to circumvent this limitation. Specifically, the solvent can be lyophilized (freeze-dried) or a super critical fluid, such as CO_2, can be used, where surface tension is not an issue. These alternative routes can, however, be impractical in an industrial setting. Dry-etching processes provide a viable alternative route to selectively remove one component. Asakawa & Hiraoka [33] first reported the use of dry O_2 RIE to remove PMMA domains, but the difference in the etching rates in PS and PMMA was small, resulting in a thin etch mask of porous PS. A more detailed analysis of the dry etching of PS-*b*-PMMA using different etching chemistry was performed by Liu *et al.* [32]. An O_2 RIE yielded an isotropic etch, while an Ar RIE resulted in an anisotropic sputtering, where 24 nm wide, 80 nm high lamellae with a pitch of approximately 50 nm were achieved (figure 3*a*). A significant drawback was that the Ar RIE severely damaged the pattern, when compared with that achieved from an O_2 RIE (figure 3*c*). Pattern transfer of the polymer mask to silicon was also achieved by using $C_2H_2F_4/SF_6$ RIE. Ting *et al.* [35] argued that an Ar/O_2 mixture gas was optimal for etching PS-*b*-PMMA in terms of both etch selectivity (2 : 1) and pattern quality. Farrell *et al.* [36] investigated the chemistry involved in CHF_3 and O_2 RIEs

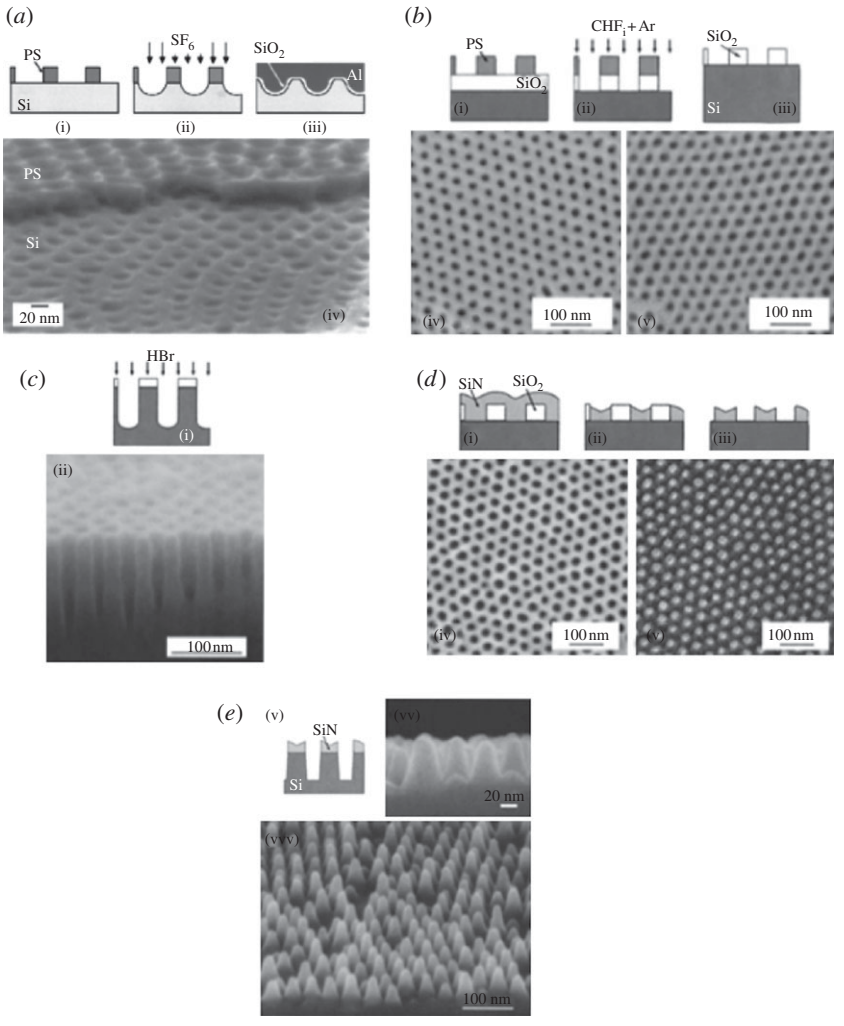

Figure 4. Examples of different pattern transfer from PS-*b*-PMMA porous templates. SEM images of (*a*) transfer of BCP pattern to silicon, (*b*) transfer of BCP pattern to SiO_2, (*c*) transfer of SiO_2 pattern to silicon, (*d*) tone reversal of the SiO_2 pattern to SiN and (*e*) transfer of SiN pattern to Si. (Adapted with permission from [37,38]. Copyright © 2001 American Institute of Physics and 2002 American Vacuum Society.)

and the selectivity in etching the PMMA domains in a PS matrix (2 : 1 etch ratio). It is interesting to note that a 3.5 : 1 etch contrast was obtained when homopolymer PS and PMMA films were investigated separately. Mixtures of SF_6 and C_4F_8 for RIE enabled a transfer of the PS mask to the underlying bulk silicon substrate [36].

Pattern transfer using a BCP template can be achieved by an addition process, where materials are deposited onto the surface covered with the BCP template, and then the BCP is removed, leaving behind negative replica of the template. Alternatively, the template can be used as a mask for etching into an underlying substrate or into a layer of active material, such as a magnetic material, creating an exact replica of the template in the active material. Black *et al.* [37] were the first to show that porous BCP templates from PS-*b*-PMMA could be used as etch masks for fluorine RIE. SF_6 RIE was used to transfer the BCP template pattern to an underlying silicon substrate (figure 4*a*), where etching into Si was 25 times more rapid than through the cross-linked PS template. The etch selectivity was much lower when the features were 30 nm or less. After the complete removal of the template, allowing a native SiO_x layer to form on the Si, and evaporating

a metal, such as Al, a semiconductor capacitor with increased charge storage capacities was produced in a straightforward manner. Guarini *et al.* [39] further investigated the conditions for template generation and showed that CHF_3 could be used as an alternative RIE gas. The hole pattern in silicon was also tone-reversed to form Si_3N_4 pillars by a three-step process. Silicon nitride was first deposited onto the SiO_2 surface having the hole pattern by thermal chemical vapour deposition (CVD). Then CH_3, CF_4, CH_2F_2 and Ar RIE were used to remove excess silicon nitride and hydrofluoric acid (HF) was then used to remove the silicon oxide template. The residual Si_3N_4 in the holes is a reverse pattern of the PS matrix that served as an etch mask for further pattern-transfer purposes (figure 4*d*). High-aspect-ratio silicon pillars were obtained by etching the Si_3N_4 mask into the underlying Si with SF_6 RIE. It should be noted that, by changing the concentration of the BCP so that there are PS cylindrical microdomains in a PMMA matrix, freestanding PS pillars covering the silicon wafer could be obtained [34]. RuO_4 was used to stain PS pillars to enhance the etch contrast so that transfer to Si_3N_4 could be achieved with CHF_3/Ar (1/9) inductively coupled plasma (ICP) RIE and, subsequently, to the silicon substrate with HBr RIE. The porous PS template has also been used as an etch mask for ion milling by Liu *et al.* [40] to transfer the BCP hole pattern to an underlying Fe layer. Although the quality of pattern transfer was poor, a bilayer of porous Fe and FeF_2 was fabricated that showed magnetic hysteresis loops and anisotropic magneto-resistance asymmetry. Similarly, fabricating a patterned magnetic metal alloy of CoCrPt nanodots via RIE and ion milling using a BCP template was shown [41]. The coercivity of the isolated CoCrPt dots was much higher than that of the continuous magnetic film. Jeong *et al.* [42] further extended the BCP lithography to a variety of other materials using PS-*b*-PMMA BCPs together with RIE and ion-milling pattern-transfer processes; for example, transferring the pattern to TiO_2 with RIE and ion milling into Pt film.

Thurn-Albrecht *et al.* [38] demonstrated the potential of BCP templates to generate very-high-aspect-ratio cobalt nanowires using an electrochemical deposition process. Here, a thick film (several tens of micrometres) of a PS-*b*-PMMA BCP with cylindrical PMMA microdomains was cast onto a silicon substrate. To orient the BCP microdomains throughout the entire film, simply modifying the interfacial interactions would not be sufficient. However, the dielectric constant difference between PS and PMMA is large enough so that an electric field could be used to induce the desired orientation of the microdomains. By placing an aluminized Kapton sheet on top of the BCP film (where a thin layer of PDMS was placed between the BCP and the Kapton to fill any air gaps) and applying a voltage across the Al and Si, an electric field is generated where the strength of the field is dictated by the separation distance between the electrodes and the dielectric constant of the BCP. It should be kept in mind that the separation distance between the electrodes is only several tens of micrometres and, as such, at low voltages, very large fields can be produced. And the fields are of sufficient magnitude to overcome interfacial interactions and orient the BCP microdomains in the direction of the applied field. Consequently, the approximately 20 nm cylindrical microdomains, which extend continuously across the film, have exceptionally high aspect ratio. Using UV radiation, the PMMA was degraded, removed by rinsing with acetic acid, leaving a nanoporous film on a silicon substrate. This was placed in an electrochemical cell where metal could easily be deposited in the pores. These authors demonstrated this method using the example of Cr, but the approach is applicable to a wide range of materials. In fact, by stopping the deposition before the pores are completely filled and transferring to another cell, one or more different materials can be deposited, producing a layered nanowire structure. One of the nice features of this deposition process is that the nanowires are embedded in an insulating polymer matrix (PS), which not only serves to isolate the nanowires from each other but also provides an inert support for the wires and stabilizes the nanowires against oxidation.

This result sparked a significant amount of research to develop the BCP templates as scaffolds for producing nanostructured materials for potential applications. Kim *et al.* [43] grew SiO_2 pillars within the BCP framework. Here, a nanoporous BCP template on a silicon substrate was placed into a stream of $SiCl_4$. In the presence of a small amount of water, SiO_x is grown at the exposed surface, i.e. within the nanopores of the BCP template. Similar chemistries can be used to produce TiO_x, where $TiCl_4$, rather than $SiCl_4$, is used. RIE was used to remove the polymeric

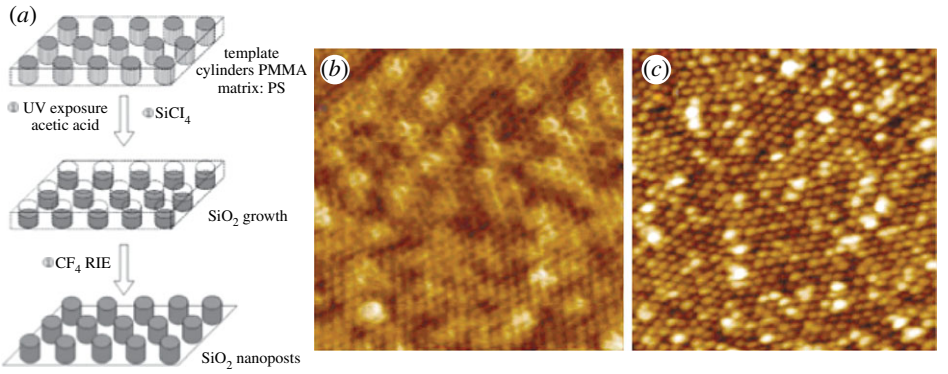

Figure 5. Example of sol–gel process to make SiO_2 pillars from a BCP template. (*a*) Schematic of the process of making SiO_2 pillars. (*b*) Atomic force microscopy (AFM) image of PS-*b*-PMMA template and (*c*) AFM height image of Si pillars. Image size $2 \times 2\ \mu m$. (Adapted with permission from [43]. Copyright © 2000 John Wiley & Sons, Inc.) (Online version in colour.)

template after the SiO_2 pillars were formed, as shown in figure 5. Calcination of a PS template with the precursor at 500°C was an alternative way of removing the polymeric template while converting the silicon precursor into SiO_x [44]. Perhaps an even simpler route to produce SiO_x nanopillars has been described previously [44–46], where a commercially available spin on glass (SOG) or tetraethoxysilane or even PDMS can be spin-coated onto the nanoporous BCP and either sol–gel chemistry or thermal treatment can produce the SiO_x that can be calcined at elevated temperatures with the organic template being removed.

A variety of metal nanostructures have also been produced by a simple metal deposition onto the nanoporous BCP template. Shin *et al.* [47] produced metal nanodots by metal evaporation, followed by a lift-off of the PS template. It is imperative, though, that the thickness of the metal deposited enables access of the solvent to the organic template for a lift-off. This method was improved by McGehee *et al.* [48], who used an obliquely angled sputter-etch to remove the metal coating on the sidewall of the polymer template, facilitating the diffusion of solvent into the polymer template. High-quality tone reversal was achieved and, subsequently, the dot pattern was transferred to the underlying Si with an NF_3 RIE, which had a 20 : 1 etch contrast between Si and Cr. This tone reversal has been used with Au immobilized in the nanopores [45] and Cr nanodots synthesized within the BCP framework [49]. Cobalt dots have been synthesized by Xiao *et al.* [49] with the combined directed self-assembly of PS-*b*-PMMA using graphoepitaxy and the lift-off process. Both Ar ion milling and oxygen RIE were used to remove excess cobalt metal and the residual PS matrix, respectively. Cobalt dots of high lateral order were templated by the BCP inside the silicon trench, as shown in figure 6.

Aside from metals, inorganic nanostructures can be grown by using the BCP template or in the nanoporous arrays. Darling and co-workers [50–54] reported a sequential infiltration synthesis (SIS) of a variety of inorganic materials using PS-*b*-PMMA templates. Trimethyl aluminium (TMA), a precursor for Al_2O_3, was selectively deposited into the PMMA domains using an atomic layer deposition (ALD) technique. TMA interacts with the carbonyl groups in the PMMA chains and creates Al-CH_3/Al-OH sites inside the PMMA scaffold. After infiltration, the BCP template was removed by O_2 RIE or by heating the film to 500°C so that Al_2O_3 lines, which replicated the BCP microdomains, remained [50]. Control over the width of the Al_2O_3 mask was achieved by varying the ALD cycle counts [50]. The SIS process improved the etching resistance of the PMMA domains by a factor of 37 by using HBr gas for the RIE [52]. The method for patterning of Al_2O_3 was extended to the patterning of other inorganic materials, including TiO_2, SiO_2, ZnO and W by using different precursors [53]. After a sufficiently long exposure to UV light the hydrophobic PS template was converted into a material with hydrophilic character. TMA was also infiltrated into the PS domains to make an Al_2O_3 mask with reversed tone [55] (figure 7).

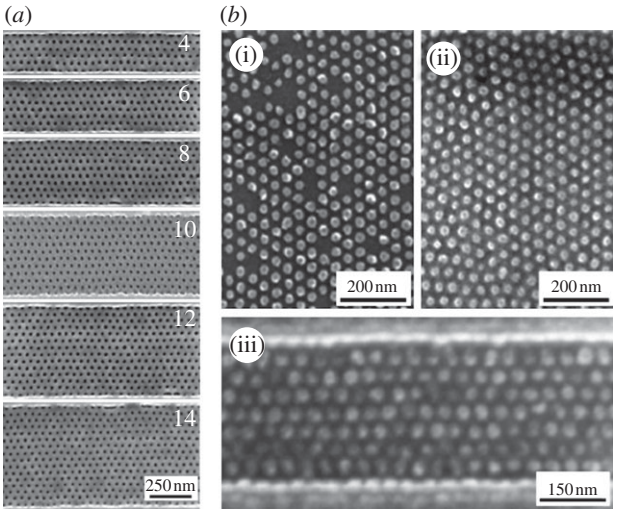

Figure 6. PS-*b*-PMMA template and cobalt dot fabrication by evaporation and subsequent lift-off. (*a*) SEM image of porous polymer template made from PS-*b*-PMMA. (*b*) SEM image of cobalt nanodots. (Reproduced with permission from [49]. Copyright © 2003 IOP publishing.)

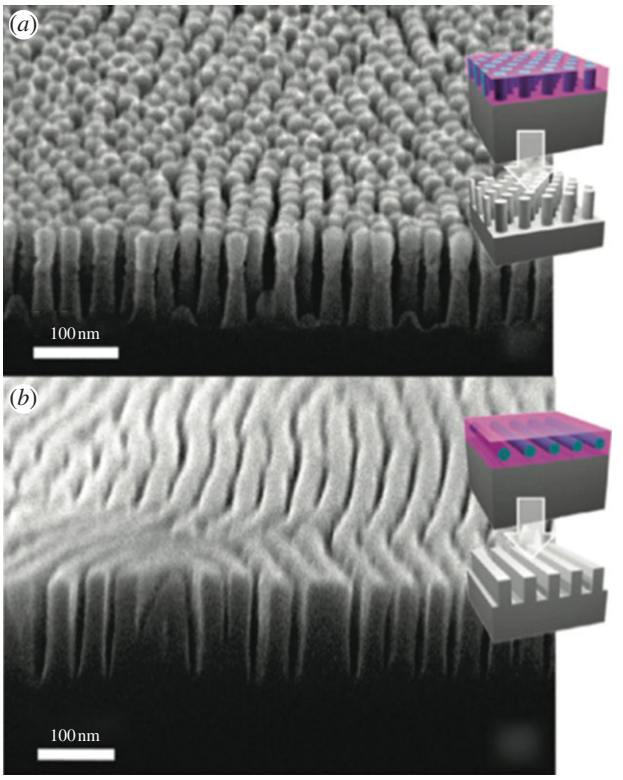

Figure 7. Example of Si patterned by PS-*b*-PMMA with SIS using an alumina oxide precursor. SEM image of (*a*) silicon pillars and (*b*) silicon trenches. (Reproduced with permission from [54]. Copyright © 2011 American Chemical Society.) (Online version in colour.)

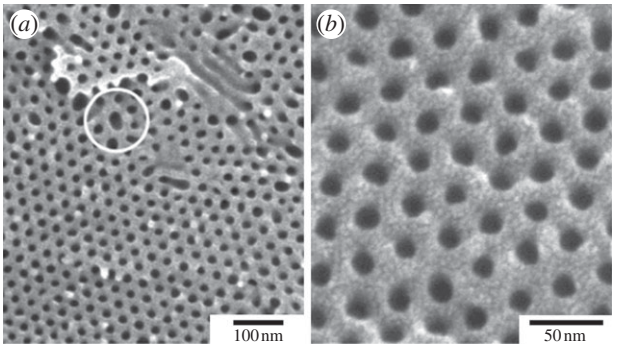

Figure 8. (*a*,*b*) SEM images of a porous polymer template after hydrolysis of PLA domains in PS-*b*-PLA. (Reproduced with permission from [61]. Copyright © 2002 American Chemical Society.)

Table 1. Flory–Huggins parameter for different BCPs.

polymer name	Flory–Huggins parameter	χ at 25°C	χ at 180°C	χ normalized by reference volume of 118 Å^3 [56]
PS-*b*-PMMA [57]	$4.46\,T^{-1} + 0.028$	~ 0.043	~ 0.038	$3.5\,T^{-1} + 0.022$
PS-*b*-PEO [58]	$29.8\,T^{-1} - 0.023$	~ 0.077	~ 0.043	$29.8\,T^{-1} - 0.023$
PS-*b*-PI [59]	$33\,T^{-1} - 0.0228$	~ 0.088	~ 0.050	$59.1\,T^{-1} - 0.071$
PS-*b*-P2VP [60]	$63\,T^{-1} - 0.033$	~ 0.178	~ 0.106	n.a.
PS-*b*-PLA [61]	$98.1\,T^{-1} - 0.112$	~ 0.217	~ 0.105	$57.4\,T^{-1} - 0.061$
PS-*b*-PDMS [58]	$68\,T^{-1} + 0.037$	~ 0.265	~ 0.187	$90.7\,T^{-1} - 0.095$
PTMSS-*b*-PLA [62]	$51.3\,T^{-1} + 0.29$	~ 0.478	~ 0.403	n.a.
PS-*b*-PFS	n.a.	n.a.	n.a.	n.a.

(ii) PS-*b*-PLA

Polystyrene-*block*-polylactide (PS-*b*-PLA) BCPs represent another interesting BCP for patterning nanostructures. PS-*b*-PLA has a large Flory–Huggins interaction parameter ($\chi \sim 0.218$ at 25°C) in comparison with PS-*b*-PMMA ($\chi \sim 0.043$), which allows a reduction of the molecular weight, while still remaining as a microphase separation and, as such, producing smaller microdomains (table 1). Zalusky *et al.* [61] systematically investigated the phase behaviour of PS-*b*-PLA by synthesizing copolymers of different molecular weights and volume fractions. Both thermal and solvent annealing was used to induce a microphase separation in PS-*b*-PLA thin films. Furthermore, the PLA microdomains in the PS-*b*-PLA BCPs can be easily removed using a weak acid or base to produce a nanoporous polymer template, as shown in figure 8. It should be noted that the template prepared in this manner is PS and is not cross-linked. This is advantageous for lift-off processes, where dissolution of the PS is easy, but it has a disadvantage in that the PS template will relax to reduce the surface area. Leiston-Belanger *et al.* [63] solved this problem by incorporating a thermally cross-linkable block of benzocyclobutene (BCB) in the PS-*b*-PLA BCP. The poly[(styrene-*r*-BCB)-*b*-lactic acid] (PSBCB-*b*-PLA) thin film sample was thermally annealed at 170°C for several hours to induce the formation of hexagonally packed PLA cylindrical microdomains. In a second annealing step, the temperature was raised to 200°C for several hours to cross-link the PS matrix. A cross-linked porous PS template was obtained after subsequent removal of the PLA domains by hydrolysis as described above.

The methods for controlling the domain orientation in PS-*b*-PLA BCPs are similar to those used for PS-*b*-PMMA BCPs. A neutral brush layer was also reported to control the domain

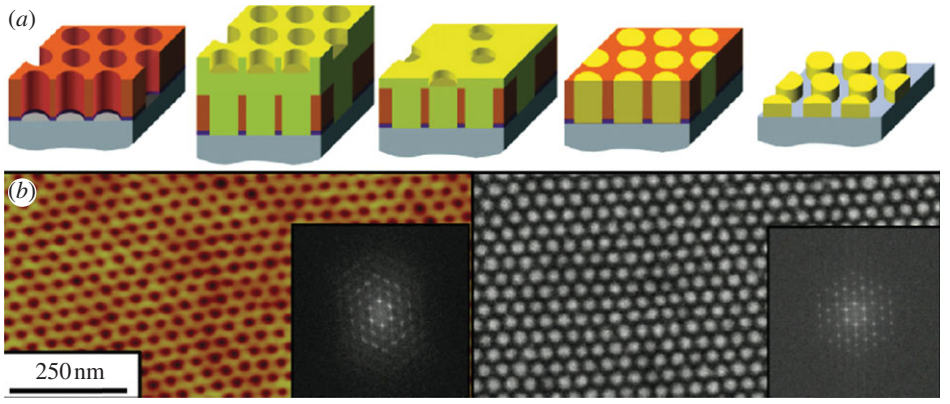

Figure 9. Magnetic $Ni_{80}Fe_{20}$ domain template generated by PS-*b*-PLA. (*a*) Schematic of the fabrication process. (*b*) AFM image of a porous polymer template and $Ni_{80}Fe_{20}$ domains. (Reproduced with permission from [67]. Copyright © 2011 American Chemical Society.) (Online version in colour.)

orientation of PS-*b*-PLA BCPs. Keen *et al.* [64] reported that the use of a random brush copolymer PS-*r*-PMMA (32–38% PS composition) allowed the lamellae in PS-*b*-PLA to be oriented normal to the substrate. Solvent annealing is an alternative way of inducing a microphase-separated state and also allows control of the orientation of the microdomains in PS-*b*-PLA BCPs. Vayer *et al.* [65] showed examples of vertically oriented pores that spanned the entire PS matrix, and were produced by annealing of the PS-*b*-PLA thin film in tetrahydrofuran (THF) vapour and subsequent removal of the PLA by hydrolysis. They also used UV light to cross-link PS in order to avoid delamination during the hydrolysis process.

The porous templates made from PS-*b*-PLA BCPs have been used in various lithography applications. For example, Olayo-Valles *et al.* [66] selectively stained the PS domains by RuO_4 vapour to increase the etch resistance to O_2 RIE. An evaporation of 5 nm $Ni_{80}Fe_{20}$ on a porous template followed by a template lift-off produced magnetic $Ni_{80}Fe_{20}$ nanodots. Baruth *et al.* [67] demonstrated the fabrication of magnetic dots by overfilling a porous PS template with $Ni_{80}Fe_{20}$ followed by Ar ion milling and etching (figure 9). A sol–gel replication method was also reported using PS-*b*-PLA BCPs. Nguyen *et al.* [68] converted a porous polymer template to the negative pattern of SiO_2 using infiltration of TOES precursors followed by thermal degradation of the polymer template.

(iii) PS-*b*-PEO

Polystyrene-*block*-poly(ethylene oxide) (PS-*b*-PEO) has emerged as another attractive candidate for nanofabrication since the Russell group in 2004 demonstrated solvent annealing in PS-*b*-PEO to produce hexagonal arrays of microdomains that are free from defects in an area of 25 μm^2 [69] (figure 10). This work sparked research interest in both the use of PS-*b*-PEO BCPs for nanofabrication and the process of solvent vapour annealing. Solvent (vapour) annealing provides an alternative annealing method for polymers, which are sensitive to thermal degradation. The procedure for solvent annealing of PS-*b*-PEO can be summarized as follows. A spin-coated PS-*b*-PEO thin film was placed inside a sealed jar with a THF reservoir. The evaporation of THF led to both a swelling and a plasticization of the PS-*b*-PEO film. The related enhanced mobility of the polymer chains facilitated the formation of ordered microdomains through a microphase separation. It is worth noting that PS-*b*-PEO has a high Flory–Huggins parameter ($\chi \sim 0.077$ at room temperature), and it is even higher if the PEO blocks were complexed with ions [2]. The current record in the area density of a polymer pattern, 10 teradot per $inch^2$, was obtained using PS-*b*-PEO, which was complexed with $HAuCl_4$ salt [2]. The

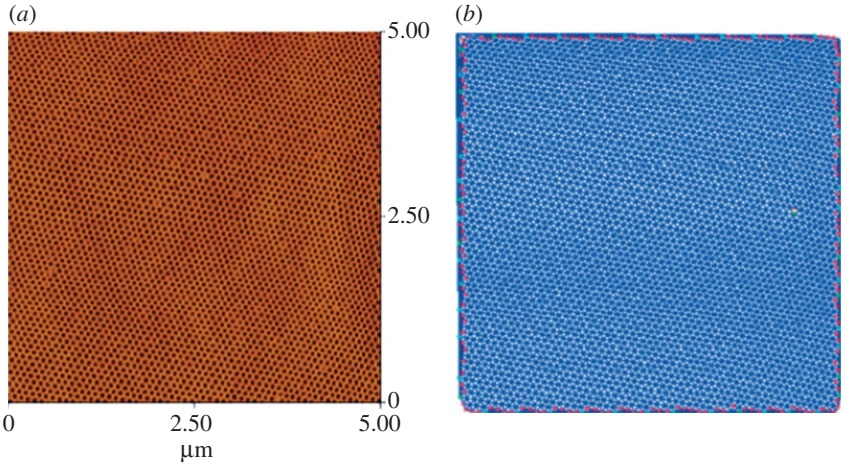

Figure 10. Highly ordered array of PEO domains in a PS-*b*-PEO BCP obtained by solvent annealing. (*a*) AFM phase image and (*b*) Voronoi diagram defect analysis. (Reproduced with permission from [69]. Copyright © 2004 John Wiley & Sons, Inc.) (Online version in colour.)

dimension of a porous polymer template can be controlled by using PS-*b*-PEO with different molecular weight and by blending with either PEO or PMMA homopolymer [70].

One of the drawbacks of PS-*b*-PEO BCPs is that, unlike PS-*b*-PMMA or PS-*b*-PLA BCPs, there is no simple way of degrading the PEO domains. However, various PS-*b*-PEO-based polymers have been synthesized to circumvent this problem. For example, Bang *et al.* [71] used reversible addition fragmentation chain transfer (RAFT) polymerization to synthesize a PS-*b*-PMMA-*b*-PEO triblock copolymer, which allows chain scission under UV light to remove the PEO domains, and thus the fabrication of a highly ordered porous PS template. Alternatively, an acid cleavable juncture, a triphenylmethyl(trityl) ether linkage, was introduced between PS and PEO to create a cleavable PS-*b*-PEO BCP [72]. Brønsted or Lewis acids at ambient conditions can readily cleave a trityl ether linkage. For example, highly ordered PEO microdomains were achieved by solvent annealing of cleavable PS-*b*-PEO in benzene vapour for 48 h. Further annealing in trifluoroacetic acid vapour was used to cleave the junction between PS and PEO domains. A methanol–water (10 : 1) solvent mixture served to rinse the degraded PS-*b*-PEO film, and dissolved the cleaved PEO domains, leaving a porous PS template for further patterning applications. *O*-nitrobenzyl ester, a photo-cleavable junction, was synthesized between PS and PEO domains by RAFT polymerization [73]. This makes PS-*b*-PEO degradable under 365 nm UV light (dose of 5.6 J cm^2), and it behaves similarly to PS-*b*-PMMA but with a higher Flory–Huggins interaction parameter. Reconstruction in a selective solvent is a convenient way of obtaining a porous polymer template of PS-*b*-PEO BCP. The use of ethanol, a good solvent for PEO but a bad solvent for PS, allows for fabrication of a hexagonally packed porous polymer template of PS-*b*-PEO [74]. In another study, it was shown that HI acid cleaves the PEO domains in PS-*b*-PEO, producing porous PS templates [75].

Porous templates fabricated from PS-*b*-PEO BCPs have been used as an etch mask for patterning of various materials. For example, Gu *et al.* [74] used a solvent-annealed and reconstructed PS-*b*-PEO mask to pattern high-aspect-ratio silicon holes using SF_6 and O_2 low-temperature RIE (etch recipe: flow rate 34 sccm SF_6 and 16 sccm O_2, RF power 1000 W, 10 mTorr pressure and a temperature of −120°C). The low-temperature etching was used to condense a passivation layer on the sidewall of the silicon, which allows an almost vertical etch profile. An etching selectivity up to 8 : 1 was obtained between the organic mask and the silicon wafer. A hexagonally packed array of 20 nm silicon holes was etched into the silicon substrate to a depth of 60 nm [74]. Moreover, other patterning methods were used related to PS-*b*-PEO porous

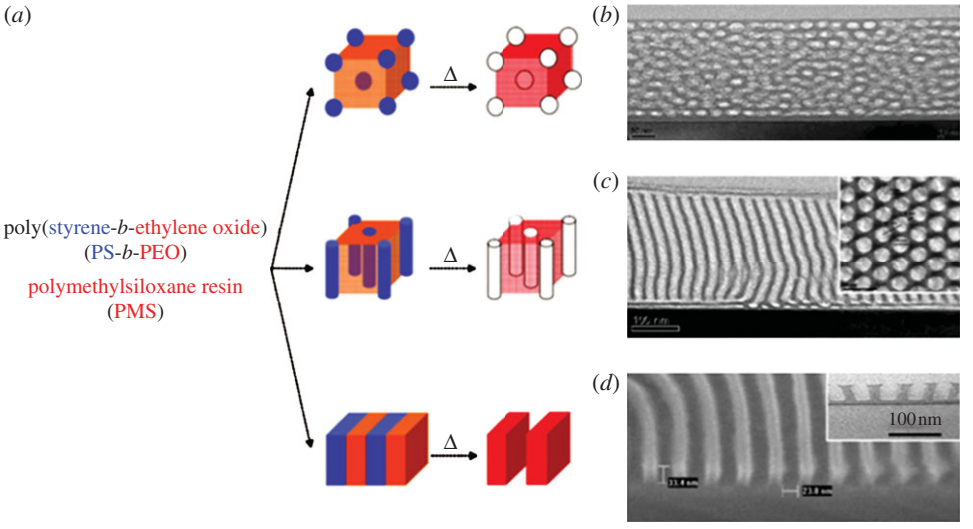

Figure 11. (*a–d*) Examples of nanostructures templated from PS-*b*-PEO co-assembly with silicon-containing PMS. (Reproduced with permission from [79]. Copyright © 2008 IOP publishing.) (Online version in colour.)

templates. For example, a selective sol–gel process was performed on the hydrophilic PEO block [76]. H_2O condensed exclusively in the PEO domains after an immersion of the PS-*b*-PEO BCP in water, which selectively reacts with $SiCl_4$ or $TiCl_4$ to generate SiO_2 or TiO_2 posts. A PDMS homopolymer, another precursor for SiO_x, was used to fabricate silicon oxide pillars [77]. A thin layer of PDMS in heptane was spin-coated onto a porous PS-*b*-PEO template. Upon heating the sample to 60°C, capillary forces drove PDMS into the porous template. O_2 RIE was used to remove the polymer template, and to convert PDMS into silicon oxide pillars. An area density up to 2 teradot per $inch^2$ was achieved using this method.

Another interesting way of enhancing the etch resistance of PEO domains is to co-assemble silicon-containing small molecules with PS-*b*-PEO BCPs [78] (figure 11). Silsesquioxane (SSQ), which contains silicon that is more resistant to etching, preferentially interacts with PEO during the self-assembly of a BCP/SSQ mixture [80]. Thermal cross-linking of the SSQ and a decomposition of the polymer template above a temperature of 450°C produced a silica nanostructure, which was a replicate of the PEO microdomain structure. Similarly, polymethylsiloxane (PMS) can be coassembled with PS-*b*-PEO BCPs to improve the etch selectivity [81]. Sundström *et al.* [82] co-assembled PMS with PS-*b*-PEO BCPs, then converted the PEO domains to SiO_2, and used CF_4 RIE to transfer a silica mask to a silicon substrate. The achieved aspect ratio of the silicon structure, however, was limited to values of 1 : 1 [82]. Park *et al.* [81] showed a strategy for patterning a porous template with a high aspect ratio by using a structure with bilayers, a PS-*b*-PEO–PMS polymer mixture and an organic transfer layer. Pores were achieved with an aspect ratio of 5 : 1 and with a depth of 25 nm in the organic transfer layer. The co-assembly of silicon-containing materials with PEO domains in PS-*b*-PEO BCPs not only improves the etch resistance of the PEO domains but also increases the unfavourable interactions between PS and PEO domains. Park *et al.* [83] reported that the spacing of microdomains was as low as 14 nm in PS-*b*-PEO BCPs with a total molecular weight of 5.1 kg mol^{-1} (PS-*b*-PEO, 3-*b*-2.1 kg mol^{-1}). In this case, the neat copolymer PS-*b*-PEO (5.1 kg mol^{-1}) did not microphase separate. DSA was used to obtain lateral ordering within hybrid systems. For example, Cheng *et al.* [84] showed that by using topographical trenches the self-assembly of lamellae in a PS-*b*-PEO/organic silica hybrid system can be directed to produce a pattern of lamellae of unidirectional orientation [84]. On the other hand, Kim *et al.* [79] found that lamellae were aligned normal to the surface in shallow silicon trenches. Both methods demonstrated that BCP/organic

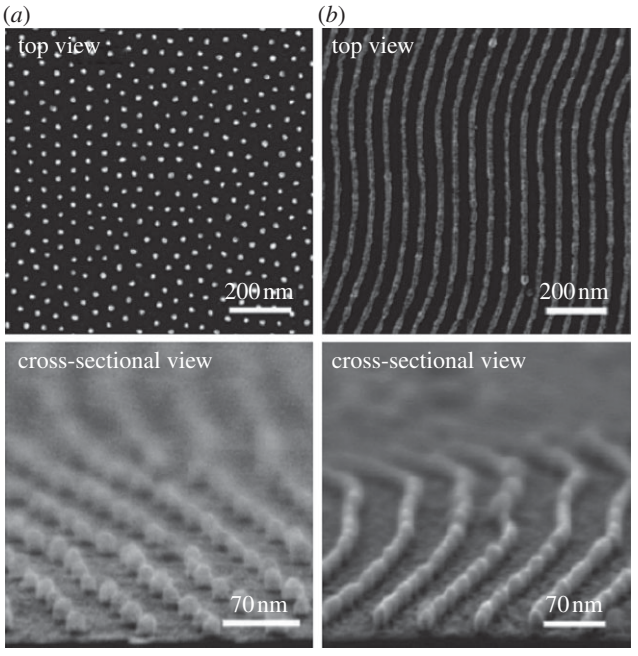

Figure 12. SEM image of a Pt mask fabricated from PS-*b*-P2VP loaded with Pt salt. (*a*) Dot patterns and (*b*) line patterns. (Reproduced with permission from [89]. Copyright © 2009 American Chemical Society.)

silica hybrids behave similarly to neat BCPs and their self-assembly can be directed when it is combined with top-down patterning techniques.

(iv) PS-*b*-P2VP and PS-*b*-P4VP

Polystyrene-*b*-poly(vinyl pyridine) (PS-*b*-PVP) represents another interesting class of polymer materials mainly because of the pyridine group in the PVP blocks. Metal counter ions can interact with the pyridine groups (actually pyridinium groups after protonation) of the PVP blocks in PS-*b*-PVP, which offers the possibility to make metal structures by reduction of coordinated metal counter ions [85,86]. Spatz *et al.* [85,86] were the first to mix PS-*b*-P2VP BCPs with chloroauric acid ($HAuCl_4$), then dip-coat the resulting films for the formation of PS-*b*-P2VP micelles complexed with gold ions. Gold domains with a size of 25 nm and a period of 45 nm were fabricated on the entire wafer. Such gold domains can serve as an excellent hard mask for pattern transfer using RIE or Ar ion milling. Chai and co-workers [87–89] further extended the use of PS-*b*-P2VP BCPs to fabricate various metal structures with line patterns. In contrast to a mixing of metal ions with BCPs beforehand, they first self-assembled the neat PS-*b*-P2VP thin film on silicon using thermal annealing (230°C for a day), then the annealed BCP film was immersed into an aqueous solution of metal ions with diluted acid to form a complex of metal ions and P2VP domains. For example, a PS-*b*-P2VP BCP thin film was immersed in a 10 mM Na_2PtCl_4/0.9% HCl solution for 3 h, then etched in O_2 RIE to remove the polymer template and to produce Pt metal lines (figure 12). Such metal masks are very robust towards various etching gases, and have the potential for pattern transfer to other functional materials.

As for PS-*b*-PEO BCPs, there is no straightforward way of selectively removing P2VP domains. But reconstruction of PS-*b*-P2VP BCPs in a selective solvent, for example ethanol, also produces a porous polymer template. Park *et al.* performed a number of different experiments on PS-*b*-P2VP and PS-*b*-P4VP diblock copolymers using solvent annealing and they used the generated patterns for lithography applications [2,28,81,90–95]. Toluene or THF was used for a solvent annealing of spin-coated PS-*b*-P2VP or PS-*b*-P4VP films to obtain highly ordered arrays of microdomains. After

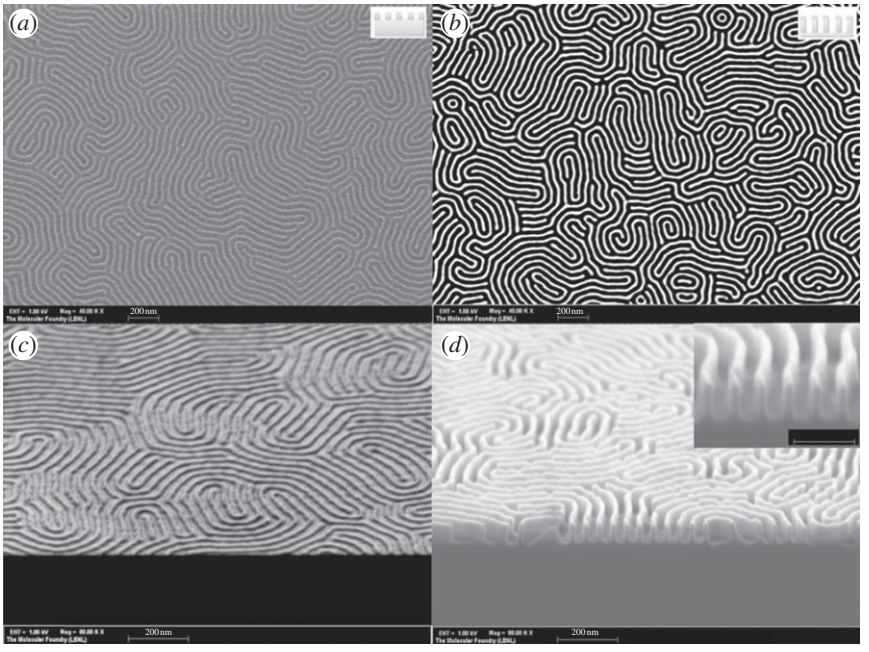

Figure 13. Silicon patterns made from a PS-*b*-P2VP BCP. (*a*,*c*) Polymer mask made from a PS-*b*-P2VP template. (*b*,*d*) Silicon fins after pattern transfer from a BCP mask. (Reproduced with permission from [96]. Copyright © 2012 John Wiley & Sons, Inc.)

a reconstruction of the film in ethanol, a highly ordered hexagonal pattern of holes was obtained in the polymer film. Similar to porous films of PS from PS-*b*-PMMA BCPs, lots of applications of polymer templates were demonstrated also in the case of PS-*b*-P2VP. Patterns of porous PS-*b*-P4VP templates were transferred to silicon oxide using RIE etching [81]. The quality of the pattern transfer from the polymer mask to silicon was greatly improved by using low-temperature RIE etching [74]. Fifteen-nanometre silicon fins with a 5 : 1 aspect ratio were patterned across a 1-inch^2 surface. The polymer mask was fabricated using the self-assembly of a PS-*b*-P2VP BCP together with reconstruction and RIE. The polymeric mask was then etched in SF_6 gas ICP RIE at −120°C (figure 13). Different metals such as gold or chrome were evaporated on the porous polymer template, followed by a lift-off to produce metal dots [28]. Silver dots were also generated from a PS-*b*-P2VP BCP by coordination of the P2VP blocks with 3 mM silver nitrate ($AgNO_3$) in a dilute HF solution. Such silver nanodots act as an etch mask for metal-assisted wet etching using HF and H_2O_2, for example, to etch into a silicon substrate and to produce silicon wires with a high aspect ratio [97,98]. Such silicon wires with a high aspect ratio greatly increase the surface area of silicon, and were reported to be used as an electrode for battery applications [97]. Alternatively, a PDMS precursor in heptane can be spin-coated onto a porous polymer template, and then reduced by RIE in order to produce silicon oxide pillars [91]. Gu *et al.* [96] further extended this method to fabricate silicon oxide pillars with a large feature size. Before spin coating of PDMS, a short-time isotropic O_2 RIE was used to enlarge the size of the pores in a PS-*b*-P2VP template. Silicon oxide pillars with a high area density of 2 teradot per inch^2 were obtained using a PS-*b*-P4VP BCP with a molecular weight of 15 kg mol^{-1}. A PS-*b*-P4VP thin film was also used as an etch mask for wet etching of a silicon wafer [99]. For the wet etching of silicon the BCP film was dipped in a dilute HF (aq) solution. The pattern of the P4VP domains was transferred to the underlying silicon. A longer etching time of silicon by HF produces holes with an increased size due to the undercut of silicon beneath the BCP pattern.

An interesting method combines both solvent annealing and thermal annealing (by using a microwave heater) and was proposed by Zhang *et al.* [100,101]. A PS-*b*-P2VP thin film was

placed in a sealed polytetrafluoroethylene (PTFE) chamber together with a solvent reservoir at the bottom. The BCP film was heated in a microwave oven and simultaneously exposed to solvent vapour. The authors found that this combined annealing method reduced the required time for producing a well-ordered microdomain structure to a minute. This method has the potential to greatly increase the throughput of BCP lithography and significantly reduce the cost of fabrication. It is also worth noting that in a structure of double-layered cylindrical domains the domain spacing can be decreased to half by loading the cylinders parallel to the substrate with a metal, and subsequently etching away the BCP template [102].

(v) Other organic block copolymers

A lot of other polymers are also worth mentioning and will be discussed here. Poly(α-methylstyrene)-*block*-poly(4-hydroxystyrene) (PαMS-*b*-PHOST) BCPs are a unique class of BCPs [103–106]. They not only are able to self-assemble into nanoscopic domains, but can also be used as negative-tone photoresist when combined with small amounts of a photoacid generator (triphenylsulfonium triflate; TPST) and a cross-linker (tetramethoxymethyl glycoluril; TMMGU) [103]. The combination of photolithography with PαMS-*b*-PHOST BCPs self-assembly results in an area-selective high-resolution BCP lithography that allows for the generation of arbitrary shapes. Organic polymer materials with a high Flory–Huggins interaction parameter were also reported. Poly(styrene-*block*-acrylic acid) (PS-*b*-PAA) BCPs were estimated to have a $\chi > 0.3$. Zhang *et al.* [107] self-assembled a PS-*b*-PAA BCP on a silicon surface, and observed a pitch of 14 nm from a neat PS-*b*-PAA BCP (5.1-*b*-3.9 kg mol^{-1}). Triblock copolymers also were developed for lithography applications. For example, a PEO-*b*-PMMA-*b*-PS ABC triblock copolymer was annealed under a high relative humidity, followed by UV degradation and acid washing. A square packing of half-spheres at the surface was observed as a result of interactions between the hydrophilic PEO segments and water vapour during processing. Such structures with square packing are very interesting from an industrial perspective [108].

(b) Block copolymers containing inorganic material

The etch contrast between the different blocks in BCPs is naturally low because they are made of organic polymers. As described above, the selective removal of one domain either by use of UV radiation or by reconstruction of the film in a selective solvent is required to produce a porous template. BCPs in which one block contains inorganic material provide an alternative for producing porous templates because they are much more resistant to O_2 RIE. By the application of O_2 RIE the organic block can be easily removed, while the slower etching rate in the inorganic block allows the necessary contrast for preparing an etch mask to be achieved. This rather simple process makes BCPs containing inorganic material attractive for lithography applications. Moreover, incorporating inorganic material into one block of a BCP increases the unfavourable interactions between the different blocks, which promises a reduction in the size of the microdomains below 10 nm. On the other hand, the drawback of using inorganic masks is that the residual inorganic mask is relatively hard to remove. In addition, residual inorganic materials have ions, which contaminate the device fabrication and reduce the performance of devices. In the following sections, some of the most commonly used BCPs that contain inorganic materials will be reviewed.

(i) PS-*b*-PDMS

Polystyrene-*block*-polydimethylsiloxane (PS-*b*-PDMS) is one of the most widely researched diblock copolymers that contain inorganic material. It has a relatively high Flory–Huggins interaction parameter that is approximately 0.26 at room temperature (table 1). An area density up to 4 teradot per inch^2 was reported for PS-*b*-PDMS patterns [109]. PDMS domains have in comparison with PS domains a high etch resistance to O_2 RIE, so that dry etching of PS-*b*-PDMS produces SiO_x masks that can be used for further pattern transfer.

The control of the orientation of microdomains in PS-*b*-PDMS is more difficult than in PS-*b*-PMMA because of the large difference in the surface energies between PS and PDMS. The silicon-containing PDMS blocks have a lower surface tension ($\gamma_{PDMS} \sim 20.4\,mN\,m^{-1}$) than PS blocks ($\gamma_{PS} \sim 40.7\,mN\,m^{-1}$) so that PDMS domains selectively segregate to the air–polymer interface during self-assembly [110]. In thin films (approx. $1\,L_0$) of PS-*b*-PDMS, a wetting layer of PDMS is formed at the air–polymer interface that can be removed by a brief CF_4 RIE, which is typically followed by an O_2 RIE to remove the PS matrix. For thicker films (approx. $10\,L_0$), PS-*b*-PDMS forms mixed morphologies throughout the whole film after annealing [110]. Although cylindrical PDMS domains were aligned parallel to the substrate close to the polymer–air interface, their orientation was normal to the substrate in the middle of the film. Such a structure is unfavourable for a pattern transfer since it prohibits a direct transfer of the PDMS pattern to the substrate by dry etching. Recently, Bates *et al.* [111] used polarity-switching top coats to control the interfacial interactions and thus the orientation of BCP domains. Polymers composed of maleic anhydride and two other components served as top coats after spin coating from basic aqueous solution in the acid salt form. Subsequent heat treatment switched the polarity of the top coats, which in turn were neutralized, enabling a perpendicular alignment of the microdomains. The top coats could be removed by rinsing the film in a polar solvent. For example, they were able to produce lamellae that were aligned normal to the substrate in both poly(styrene-*block*-trimethylsilylstyrene-*block*-styrene) and poly(trimethylsilylstyrene-*block*-lactide) BCPs by a simple thermal annealing of the films [111]. This method enables the generation of silicon-containing masks with high aspect ratio for patterning sub-10 nm features while avoiding a wetting PDMS layer at the polymer–air interface.

The Ross group performed detailed studies of PS-*b*-PDMS BCPs for DSA, pattern transfer and device fabrication [112]. Jung *et al.* [112] were the first to demonstrate the lithography application of PS-*b*-PDMS BCPs in thin films. A PS-*b*-PDMS BCP with a molecular weight of $44.5\,kg\,mol^{-1}$ was first spin-coated onto a silicon wafer, then solvent annealed in toluene vapour for microphase separation, and finally etched by using CF_4 and O_2 RIE to produce a SiO_x etch mask. Further pattern transfer from the SiO_x mask to the underlying silica substrate was demonstrated by using CF_4 RIE. In a different method metals were evaporated on the BCP template to fabricate metal masks (figure 14) [113–116]. For example, metals such as Co, Pt, W, Ta and Ni were first sputtered on SiO_x, which was made from PS-*b*-PDMS. After the deposition of a relatively thick film, for example 55 nm, the deposited metal layer on the top of the polymer mask was partially planarized. CF_4 RIE was used for etching both the planarized metal and the SiO_x mask. Metal layers were formed because metals have a much slower etch rate than SiO_x during CF_4 RIE. For example, 9-nm-wide W wires were produced using the methodology described above [116]. Furthermore, DSA was applied to the PS-*b*-PDMS BCP to generate unidirectional metal line patterns [115] or hexagonally ordered metal dot arrays [114]. The metal patterns were also used as hard masks for further pattern transfer to the underlying SiO_2 substrate [115].

PDMS-based triblock copolymers were also reported. For example, PS-*b*-PDMS-*b*-PLA was shown to self-assemble into core shell cylinders oriented normal to the sample surface [117]. PDMS was located in the middle of the ring, and thus etching by oxygen plasma served to remove the organic material leaving behind a silicon oxide ring pattern. By using Ar ion beam milling the silicon oxide rings were also transferred to other materials including Au, $Ni_{80}Fe_{20}$ and $Ni_{80}Cr_{20}$.

(ii) PFS-containing block copolymers

Polystyrene-*block*-poly(ferrocenyldimethylsilane) (PS-*b*-PFS) are BCPs that contain both silicon and iron in one of the blocks of the copolymer. By using O_2 RIE, the PFS domains can be oxidized to form non-volatile metal oxides, which lead to relatively low etching rates compared with organic polymers [118]. Homopolymer thin films of PS and PFS showed an etching contrast up to 40 : 1 [118]. However, metal ions from the PFS domains contaminate transistor devices and thus limit patterning applications of PFS-containing BCPs.

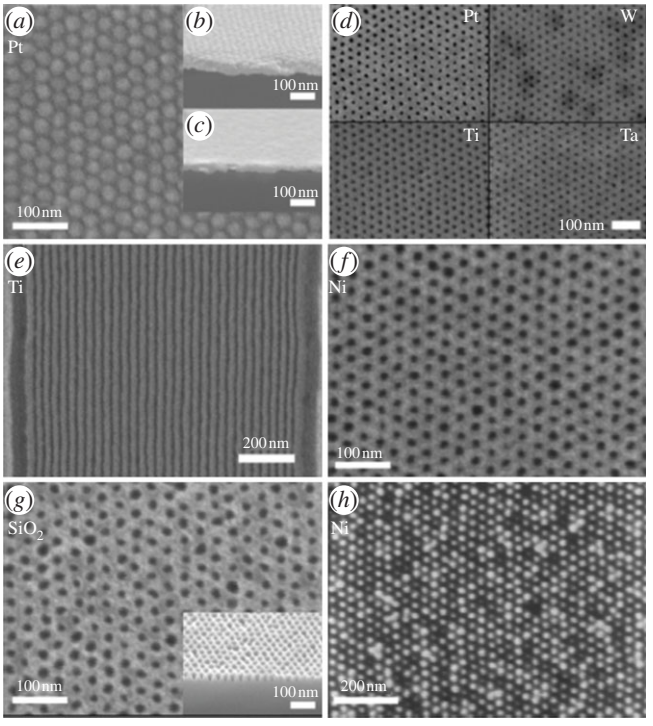

Figure 14. (*a–h*) Various metal nanostructures (as indicated in the corner of respective images) made from PS-*b*-PDMS BCP templates. (Reproduced with permission from [113]. Copyright © 2009 John Wiley & Sons, Inc.)

Both thermal and solvent annealing facilitates the microphase separation of PS-*b*-PFS BCPs. For example, thermal annealing of PS-*b*-PFS thin films between 120°C and 170°C over several days induced microphase separation [119,120]. Ordered microdomains were also reported for PI-*b*-PFS diblock copolymer films directly after spin coating from a 1% toluene solution without further annealing. O_2 RIE was employed to remove the PI blocks and thereby produce an inorganic oxide mask [121]. Besides O_2 RIE, heating the sample to more than 600°C was also used to degrade the BCP and to remove the organic components [122,123]. Prior to the heat treatment, the BCP was exposed to UV light to cross-link the PS matrix and thus to prevent the flow of the matrix. Solvent vapour annealing of PS-*b*-PFS was reported under saturated toluene vapour. Control over the orientation of PFS domains was found to be strongly influenced by the thickness of the copolymer films [124,125].

Several lithography applications have been demonstrated for PS-*b*-PFS BCPs. Cheng *et al.* [126] used PS-*b*-PFS BCPs for patterning of magnetic domains. A complicated four-layer structure (from top to bottom: 50 nm PS-*b*-PFS, 30 nm silica, 15 nm tungsten, 8 nm cobalt) was used to fabricate cobalt dots. Several steps of dry etching, including O_2 RIE, CF_4 RIE and Ar ion milling, were carried out at different stages of the pattern-transfer process. The final structure of magnetic cobalt dots has the potential for data storage applications, spurring the interest for the development of bit-patterned media. PS-*b*-PFS BCPs served together with metal-assisted chemical etching for patterning silicon with high aspect ratio. PFS patterns were first transferred to SiO_2 by using CF_4 RIE and subsequently a gold layer with a thickness of 12 nm was evaporated on silicon oxide pillars. The lift-off of the pillars was realized using HF etching, wherein a gold mask remained on top of the pillars. The gold mask was etched using 10 wt% HF and 1.5 wt% H_2O_2 aqueous solution for 15 min. Silicon nanowires with ultra-high aspect ratio up to 220 : 1 (20 nm diameter, 4400 nm height) were obtained [127] (figure 15).

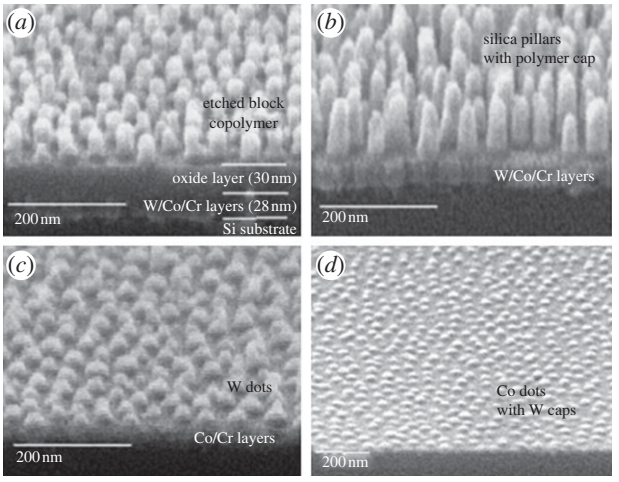

Figure 15. SEM images illustrating a nanolithography application of PS-*b*-PFS through different steps of etching. (*a*) Oxidized PFS pillars, (*b*) silica pillars with polymer cap, (*c*) W nanodots and (*d*) Co nanodots with W caps. (Reproduced with permission from [126]. Copyright © 2009 John Wiley & Sons, Inc.)

Besides diblock copolymers, triblock copolymers were also used for lithography applications because they can self-assemble into more complicated structures [128,129]. Polystyrene-*b*-polyferrocenylsilane-*b*-poly(2-vinylpyridine) (PS-*b*-PFS-*b*-P2VP) triblock copolymers, with volume fractions of 16%, 28% and 56%, respectively, have been reported to self-assemble into a cylindrical core–shell structure with PS cores and PFS shells in a P2VP matrix [130]. This novel structure enables the fabrication of inorganic ring arrays after removal of PS and P2VP. Chuang *et al.* [131] reported the formation of arrays of PFS domains with square symmetry after solvent annealing of thin films of polyisoprene-*b*-polystyrene-*b*-polyferrocenylsilane (PI-*b*-PS-*b*-PFS) triblock copolymers with volume fractions of 25%, 65% and 10%, respectively, and a subsequent transfer of the PFS pattern to a silica substrate by using RIE (figure 16). Moreover, the DSA of triblock copolymers was demonstrated by using e-beam patterned hydrogen silsesquioxane (HSQ) pillars [132]. PI-*b*-PS-*b*-PFS triblock copolymer formed interesting morphologies when it was reconstructed in a selective solvent. For example, square arrays of PI domains were converted to hole patterns after reconstructing the copolymer film in hexane, which is a good solvent for PI and a poor solvent for PS and PFS. Such square-symmetry patterns could potentially be further transferred by using deposition of metals [133] (table 2).

(iii) Other silicon-containing block copolymers

With the advance of synthetic chemistry, lots of new silicon-containing polymers have been reported. Both polymer chemists and physicists are pushing the limits of BCP lithography to achieve sub-10 nm resolution. Polyhedral oligomeric silsesquioxane (POSS) can be incorporated into BCPs by means of various methods. Hirai *et al.* [134] recently reported the fabrication of SiO_x etch masks from lamellae-forming polystyrene-*block*-poly(methyl methacrylate hedral oligomeric silsesquioxane) (PS-*b*-PMAPOSS) and cylinder-forming poly(methyl methacrylate)-*block*-poly(methyl methacrylate hedral oligomeric silsesquioxane) (PMMA-*b*-PMAPOSS) BCPs by using a one-step O_2 RIE [134]. PMMA-*b*-PMAPOSS of a total molecular 14.9 kg mol^{-1} formed a spherical morphology of PMMA domains in a PMAPOSS matrix with a periodicity of 12.4 nm [135]. POSS can also be incorporated into BCPs via click chemistry. For example, polystyrene-*b*-poly(g-propargyl-L-glutamate-*g*-polyhedral oligomeric silsesquioxane) [PS-*b*-(PPLG-*g*-POSS)]

Table 2. Chemical structure of various BCPs.

polymer name	chemical structure
PS-*b*-PMMA	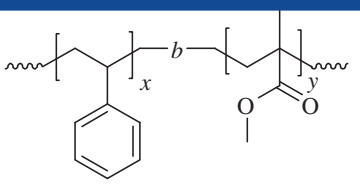
PS-*b*-PEO	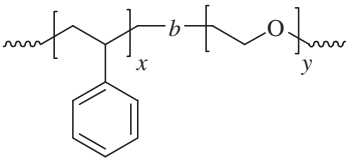
PS-*b*-PI	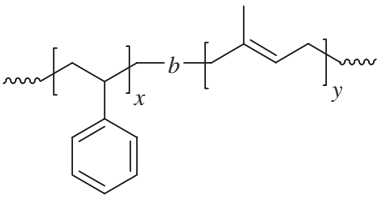
PS-*b*-P2VP	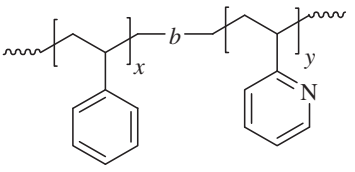
PS-*b*-PLA	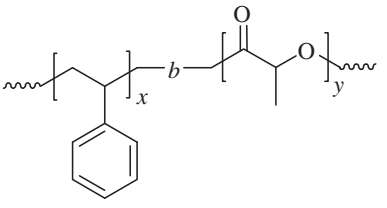
PS-*b*-PDMS	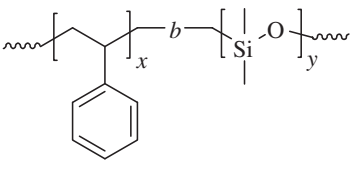
PTMSS-*b*-PLA	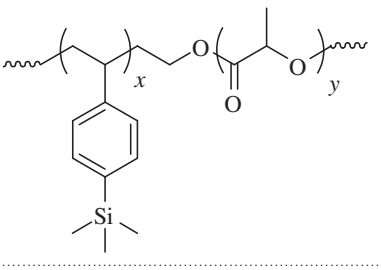
PS-*b*-PFS	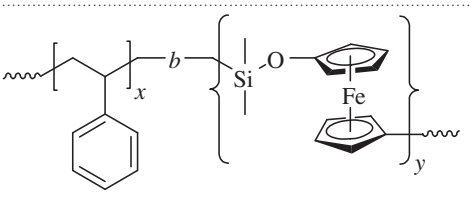

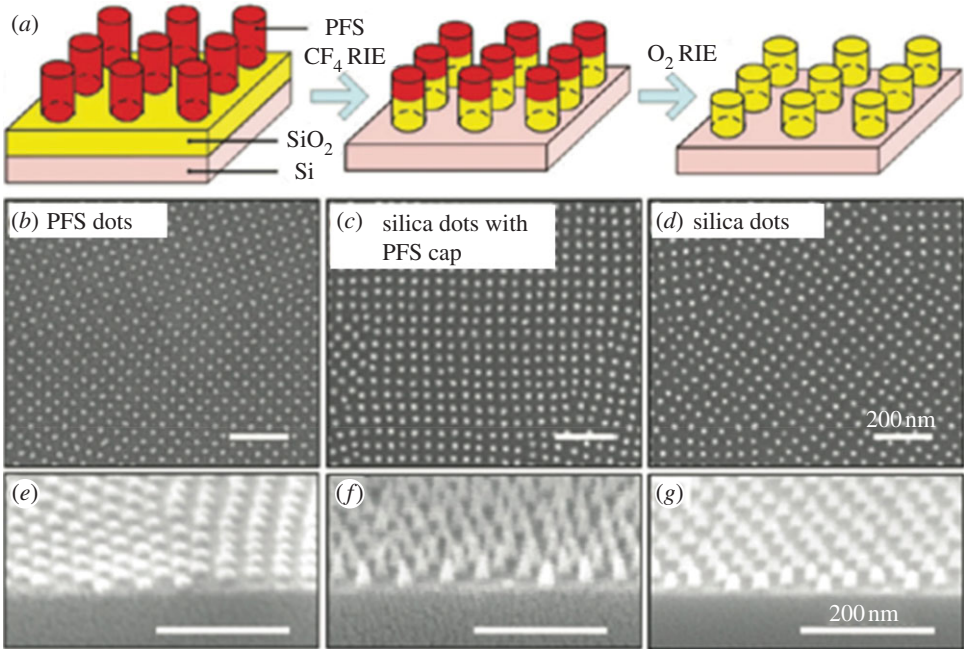

Figure 16. (*a*) SEM images of square-packed PFS domains made from a triblock copolymer and its pattern transfer to silica. (*b*,*e*) Oxidized PFS nanodots. (*c*,*f*) Silica dots with PFS cap. (*d*,*g*) Silica dots. (Reproduced with permission from [131]. Copyright © 2009 American Chemical Society.) (Online version in colour.)

was synthesized by click chemistry using PS-*b*-PPLG and N_3–POSS. PS-*b*-(PPLG-*g*-POSS) showed a morphology of cylindrical PPLG-*g*-POSS domains with a centre-to-centre distance of 10.5 nm [136].

Polysaccharide-based BCPs have also been reported to self-assemble into sub-10 nm structures as a result of the strong incompatibility between saccharidic and synthetic polymer blocks. Otsuka *et al.* [137] synthesized BCPs of maltoheptaose (MH) and poly(ε-caprolactone) (PCL) by click chemistry, and thermally annealed the BCP to form structures with feature sizes of 10 nm. Other saccharide-containing diblock copolymers composed of poly(para-trimethyl silylstyrene) (PTMSS) and oligosaccharides were synthesized through azide alkyne 'click' chemistry [138]. A feature size as small as 5 nm and a periodicity of 8.3 nm were obtained for MH-*b*-PTMSS BCPs.

Ku *et al.* [139] synthesized polystyrene-*block*-poly(4-(tert-butyldime-thylsilyl)oxystyrene) (PS-*b*-PSSi) BCPs by means of living anionic polymerization. For example, a PS-*b*-PSSi BCP with a total molecular weight of 40.6 kg mol^{-1} was found to self-assemble into PS cylinders with a diameter of 20 nm and a periodicity of 35 nm that were embedded in a PSSi matrix. O_2 RIE was employed to convert the BCP structure to an SiO_x hole pattern. The incompatibility of poly(2-vinylpyridine-*block*-dimethylsiloxane) (P2VP-*b*-PDMS) BCPs is even higher than that in PS-*b*-PDMS BCPs, which facilitated a further reduction of the feature size to 5 nm by means of solvent annealing. Moreover, the authors reported that both the size and the periodicity of the PDMS domains could be tuned depending on the degree of swelling during solvent vapour annealing [140]. A polyallyltrimethylsilane-*block*-poly(methyl methacrylate) (sPATMS-*b*-PMMA) BCP was prepared by using an α-bromoester-terminated sPATMS macroinitiator, which was chain extended by MMA using a cuprous halide-based atom transfer radical polymerization (ATRP) [141]. Poly(trimethylsilylisoprene-*b*-styrene) (PTMSI-*b*-PS) and poly(trimethylsilylstyrene-*b*-D,L-lactide) (PTMSS-*b*-PLA) were synthesized as alternative silicon-containing BCPs [62,142]. PTMSS-*b*-PLA (5.5-*b*-3.7 kg mol^{-1}) was shown to phase separate into a morphology with a period

of 12.1 nm after annealing the film in cyclohexane [62]. PLA-*b*-PDMS is another candidate to obtain small feature sizes since its incompatibility also is larger than that of PS-*b*-PDMS. Based on the calculations of the interaction parameter between PLA and PDMS, feature sizes as small as 3.5 nm were predicted for PLA-*b*-PDMS-PLA (0.6-*b*-1.0-*b*-0.6 kg mol^{-1}) triblock copolymers [143].

3. Control of orientation and lateral ordering in block copolymers

Key to the use of BCPs for BCP lithography is controlling the orientation and lateral order of the microdomains in thin films. Here, we only briefly introduce the most popular ways of controlling the orientation and lateral ordering of BCPs. For more in-depth reviews about this topic, we refer the reader to other reviews [8,144,145].

The orientation of microdomains is critical for BCP lithography applications. For the dry-etching process, the depth of patterns transferred from a mask is limited by the mask thickness and the selectivity of the specific etch recipe. Perpendicular oriented cylinders or lamellae have a high aspect ratio and are thus favoured for pattern-transfer applications. Unfortunately, a perpendicular orientation of BCP microdomains is not favoured by Nature because of the different surface energies of the two blocks of the copolymer at both the air–polymer and the substrate–polymer interfaces. For example, PMMA cylinders or lamellae in PS-*b*-PMMA BCPs prefer a parallel orientation to the surface of a silicon wafer owing to the preferential interactions of PMMA with the Si-OH at the substrate surface. Russell and co-workers [24] used a brush layer, which has neutral surface energy for both PS and PMMA, to control the orientation of PMMA microdomains. A random PS-*r*-PMMA copolymer with a hydroxyl end group was anchored to the substrate in order to adjust the surface energy of the silicon substrate. This method, however, requires the hydroxyl group to be located on the substrate, whereby the application of a hydroxyl-terminated neutral brush layer is restricted. The Russell group further improved this method by using a thermally cross-linkable random copolymer brush [146]. A random brush copolymer was spin-coated and thermally cross-linked to produce a neutral surface, making it universally applicable to any substrate. Apart from controlling the surface energy at the polymer–substrate interface, a modification of the polymer–air interface was demonstrated by using top coats for BCP thin films [111]. PDMS has a much lower surface energy than PS, thus a wetting PDMS layer segregates to the air–polymer interface after thermal annealing of PS-*b*-PDMS BCPs. Top coats, which aimed to balance the surface energies for PS and PDMS, were spin-coated on the BCP film using the cross solvent. A polymer containing a maleic anhydride moiety was designed, which, upon heating, switched its polarity to create a neutral surface for silicon-containing BCPs. Alternatively, external fields can be used to force the orientation of microdomains in a specific direction. The Russell group demonstrated field-induced alignment of microdomains in PS-*b*-PMMA BCP thin films in the presence of electric fields [23]. Solvent vapour annealing [69] was also reported to orient microdomains normal to the substrate.

Lateral ordering of the BCP microdomains is also important for some applications; for example, bit-patterned media for data storage, which requires near-perfect orientational and translational order. The merging of 'bottom-up' DSA with 'top-down' patterning techniques can potentially enable such control. Graphoepitaxy, which uses topographic features on the surfaces to bias the lattice orientation of the copolymer microdomains, has been used to bias the orientation of hexagonal lattices. For example, Segalman *et al.* [147] demonstrated the self-assembly of a single grain of PS-*b*-P2VP on a patterned silicon substrate. Various research groups have driven the progress of using topographic patterning to physically constrain BCPs tremendously. The Russell group extensively studied the self-assembly of both PS-*b*-PEO and PS-*b*-PVP BCPs on different topography patterns [2,92,148,149]. Among them, reconstructed faceted sapphire substrates have the ability of directing the self-assembly of microdomains to form arrays with long-range ordering. This approach, which relies on a crystal surface reconstruction, yet another self-assembly process, does not require large area 'top-down' lithography and shows promise as a

low-cost approach for roll-to-roll-type processes. Ross and co-workers [81,150–153] investigated PS-*b*-PFS and PS-*b*-PDMS BCPs with topography confinement. They used e-beam lithography to pattern HSQ pillars with the desired spacing and shape. Those HSQ pillars, coated with a PDMS brush, showed great capability of directing the self-assembly of PDMS microdomains. Other groups worked with various other polymers and also contributed greatly to this field. Chemical epitaxy is another way of directing the self-assembly and of controlling the lateral ordering of BCPs. Early studies were performed on PS-*b*-PMMA BCPs on alternating stripes of gold (hydrophobic) and SiO_2 (hydrophilic) produced by grazing incidence thermal evaporation of gold on a faceted Si wafer surface [154]. Chemical epitaxy also uses e-beam lithography to pattern the substrate surface with nanoscale features and provides substrates with chemical contrast. Nealey and co-workers [155–157] demonstrated the versatility and power of chemically patterned surfaces to the DSA of BCPs in a series of elegant studies. Non-symmetrical structures using lithographically defined chemical patterns, such as 90° bent line, were shown to direct the self-assembly of PS-*b*-PMMA [155]. Also, lithographically defined chemical surface patterns with frequencies over twice as much as the BCP period were used to direct the lateral ordering of BCPs by the so-called density multiplication [157].

4. Summary and outlook

Ever since the first application of BCP lithography for patterning of nanostructures in 1997, enormous progress has been made in this area. BCP lithography has now established itself as a viable strategy for patterning nanostructures. The areal density of BCP microdomains has been improved by a factor of 25 to 10 teradots per inch^2, and a resolution as small as 3 nm was achieved [2]. Precise control over orientation and lateral ordering of BCP domains was achieved by using both brush layers and DSA. Recently, the DSA of BCPs has been recognized as a promising route for future patterning technologies in the International Technology Roadmap for Semiconductors (ITRS) [1]. BCP lithography not only finds its application in the silicon conductor industry [7], but also shows a variety of other potential applications, such as bit-patterned media applications [158], antireflective coatings [159], patterning graphene transistors [160], biosensors [161] or surface-enhanced Raman spectroscopy (SERS) [162]. Overall, BCP lithography has now proved to be a powerful nanoscale patterning technique along with other patterning techniques. There are still, though, many challenges ahead that need to be addressed before BCP lithography can be integrated into industrial processes.

First, in order to advance BCP lithography to the sub-10 nm regime, new materials with high Flory–Huggins interaction parameter χ and high etch resistance need to be designed and synthesized. Reducing the molecular weight of the BCP is a typical means to increase the resolution of BCP lithography. However, χN, the incompatibility between the blocks, is required to be larger than 10.5 in order to maintain a microphase-separated structure according to mean-field theory. This limits low-χ BCPs such as PS-*b*-PMMA ($\chi \sim 0.043$) to form ordered structures with minimal periods of 20 nm. In addition, a large unfavourable interaction between two blocks reduces the interfacial thickness between the different blocks, thus reducing the line-edge roughness of the BCP. Equally important is that the etch resistance of the mask needs to be improved. Reducing the size of the mask reduces the thickness of the mask at the same time, since both quantities scale with the period of the BCP domains. Therefore, an etching recipe needs to be developed that provides a high selectivity between the polymer mask and the material to which the pattern is being transferred. A sub-10 nm dry-etching pattern transfer remains a challenge owing to a significantly slower diffusion of gas ions that are confined to nanoscopic space.

The defect density in ordered BCP patterns must not exceed 0.01 defects cm^{-2} at the resist level for all device types according to ITRS [1], which requires BCPs to phase separate and to reduce defects within a reasonable amount of annealing time. Understanding the origin of the formation of defects and methods to annihilate defects in BCP thin films is important.

Experimental results showed that an extension of thermal or solvent annealing time reduces the defect density. But systematic studies of both the thermal and solvent annealing are necessary to obtain a complete understanding of the ordering process. This would allow optimizing the processing conditions for BCP lithography in order to compete with optical lithography. Typically, in the case of photolithography, it takes only seconds to expose and develop a mask resist, and a structure can be obtained that is nearly defect-free on the whole wafer scale. So far, both solvent and thermal annealing have not reached such perfection in terms of processing time and defect density. However, a combination of both thermal and solvent annealing may provide a possibility to greatly enhance chain mobility, and thus reduce the time for DSA with minimal defects.

Third, complex integrated circuit (IC) structures, such as bends and joints, still remain a challenge for BCP lithography. However, progress has been made using the DSA of BCPs on either topography or chemistry contrast. For example, BCPs blended with homopolymers were shown to form a sharp bend structure [155]; the assembly of complex PS-*b*-PDMS patterns has been directed using HSQ pillars, which were patterned by e-beam lithography [153]. Using BCP lithography to generate even more complex three-dimensional structures has not yet been extensively explored. Intel recently introduced the 'tri-gate transistor technology', taking device fabrication into three dimensions. The use of BCPs that consist of multiple blocks has the potential to create complex three-dimensional structures [163].

Although there are still challenges to be overcome before the incorporation of BCPs into the semiconductor manufacturing process, tremendous progress has been made in the past decades. Continued research holds promise for an exciting future for the DSA of BCPs in two- and three-dimensional configurations.

Funding statement. This work was supported by the US Department of Energy BES under contract no. BES-DE-FG02-96ER45612, and by the US Department of Energy under contract no. DE-AC02-05CH11231. X.G. acknowledges the ALS Doctoral Fellowship programme for providing partial financial support. I.G. acknowledges the support of the ALS Postdoctoral Fellowship programme.

References

1. ITRS. 2011 International technology roadmap for semiconductors. See http://www.itrs.net.
2. Park S, Lee DH, Xu J, Kim B, Hong SW, Jeong U, Xu T, Russell TP. 2009 Macroscopic 10-terabit-per-square-inch arrays from block copolymers with lateral order. *Science* **323**, 1030–1033. (doi:10.1126/science.1168108)
3. Galatsis K *et al*. 2010 Patterning and templating for nanoelectronics. *Adv. Mater.* **22**, 769–778. (doi:10.1002/adma.200901689)
4. Segalman RA. 2005 Patterning with block copolymer thin films. *Mater. Sci. Eng. R-Rep.* **48**, 191–226. (doi:10.1016/j.mser.2004.12.003)
5. Hawker CJ, Russell TP. 2005 Block copolymer lithography: merging 'bottom-up' with 'top-down' processes. *MRS Bull.* **30**, 952–966. (doi:10.1557/mrs2005.249)
6. Cheng JY, Ross CA, Smith HI, Thomas EL. 2006 Templated self-assembly of block copolymers: top-down helps bottom-up. *Adv. Mater.* **18**, 2505–2521. (doi:10.1002/adma.200502651)
7. Black CT, Ruiz R, Breyta G, Cheng JY, Colburn ME, Guarini KW, Kim HC, Zhang Y. 2007 Polymer self assembly in semiconductor microelectronics. *IBM J. Res. Dev.* **51**, 605–633. (doi:10.1147/rd.515.0605)
8. Bang J, Jeong U, Ryu DY, Russell TP, Hawker CJ. 2009 Block copolymer nanolithography: translation of molecular level control to nanoscale patterns. *Adv. Mater.* **21**, 4769–4792. (doi:10.1002/adma.200803302)
9. Kim H-C, Park S-M, Hinsberg WD. 2010 Block copolymer based nanostructures: materials, processes, and applications to electronics. *Chem. Rev.* **110**, 146–177. (doi:10.1021/cr900159v)
10. Hamley IW. 2009 Ordering in thin films of block copolymers: fundamentals to potential applications. *Prog. Polym. Sci.* **34**, 1161–1210. (doi:10.1016/j.progpolymsci.2009.06.003)
11. Krausch G. 1995 Surface induced self assembly in thin polymer films. *Mater. Sci. Eng. R-Rep.* **14**, 1–94. (doi:10.1016/0927-796X(94)00173-1)

12. Meier DJ. 1969 Theory of block copolymers. I. Domain formation in A-B block copolymers. *J. Polym. Sci. C-Polym. Symp.* **26**, 81–98. (doi:10.1002/polc.5070260106)
13. Helfand E, Wasserman ZR. 1976 Block copolymer theory. IV. Narrow interphase approximation. *Macromolecules* **9**, 879–888. (doi:10.1021/ma60054a001)
14. Leibler L. 1980 Theory of microphase separation in block copolymers. *Macromolecules* **13**, 1602–1617. (doi:10.1021/ma60078a047)
15. Hong SW, Voronov DL, Lee DH, Hexemer A, Padmore HA, Xu T, Russell TP. 2012 Controlled orientation of block copolymers on defect-free faceted surfaces. *Adv. Mater.* **24**, 4278–4283. (doi:10.1002/adma.201201279)
16. Voronov DL *et al.* 2010 High-efficiency 5000 lines/mm multilayer-coated blazed grating for extreme ultraviolet wavelengths. *Opt. Lett.* **35**, 2615–2617. (doi:10.1364/OL.35.002615)
17. Mansky P, Chaikin P, Thomas EL. 1995 Monolayer films of diblock copolymer microdomains for nanolithographic applications. *J. Mater. Sci.* **30**, 1987–1992. (doi:10.1007/BF00353023)
18. Mansky P, Harrison CK, Chaikin PM, Register RA, Yao N. 1996 Nanolithographic templates from diblock copolymer thin films. *Appl. Phys. Lett.* **68**, 2586. (doi:10.1063/1.116192)
19. Park M, Harrison C, Chaikin PM, Register RA, Adamson DH. 1997 Block copolymer lithography: periodic arrays of $\sim 10^{11}$ holes in 1 square centimeter. *Science* **276**, 1401–1404. (doi:10.1126/science.276.5317.1401)
20. Harrison C, Park M, Chaikin PM, Register RA, Adamson DH. 1998 Lithography with a mask of block copolymer microstructures. *J. Vac. Sci. Technol. B* **16**, 544–552. (doi:10.1116/1.589860)
21. Li RR, Dapkus PD, Thompson ME, Jeong WG, Harrison C, Chaikin PM, Register RA, Adamson DH. 2000 Dense arrays of ordered GaAs nanostructures by selective area growth on substrates patterned by block copolymer lithography. *Appl. Phys. Lett.* **76**, 1689–1691. (doi:10.1063/1.126137)
22. Park M, Chaikin PM, Register RA, Adamson DH. 2001 Large area orientation of block copolymer microdomains in thin films via directional crystallization of a solvent. *Appl. Phys. Lett.* **79**, 257. (doi:10.1063/1.1378046)
23. Morkved TL, Lu M, Urbas AM, Ehrichs EE, Jaeger HM, Mansky P, Russell TP. 1996 Local control of microdomain orientation in diblock copolymer thin films with electric fields. *Science* **273**, 931–933. (doi:10.1126/science.273.5277.931)
24. Mansky P, Liu Y, Huang E, Russell TP, Hawker C. 1997 Controlling polymer–surface interactions with random copolymer brushes. *Science* **275**, 1458–1460. (doi:10.1126/science.275.5305.1458)
25. Thurn-Albrecht T, Steiner R, DeRouchey J, Stafford CM, Huang E, Bal M, Tuominen M, Hawker CJ, Russell TP. 2000 Nanoscopic templates from oriented block copolymer films. *Adv. Mater.* **12**, 787–791. (doi:10.1002/(SICI)1521-4095(200006)12:11<787::AID-ADMA787>3.0.CO;2-1)
26. Xu T, Stevens J, Villa JA, Goldbach JT, Guarini KW, Black CT, Hawker CJ, Russell TP. 2003 Block copolymer surface reconstruction: a reversible route to nanoporous films. *Adv. Funct. Mater.* **13**, 698–702. (doi:10.1002/adfm.200304374)
27. Xu T *et al.* 2004 Scattering study on the selective solvent swelling induced surface reconstruction. *Macromolecules* **37**, 2972–2977. (doi:10.1021/ma0355204)
28. Park S, Wang J-Y, Kim B, Russell TP. 2008 From nanorings to nanodots by patterning with block copolymers. *Nano Lett.* **8**, 1667–1672. (doi:10.1021/nl0805110)
29. Jeong U, Kim HC, Rodriguez RL, Tsai IY, Stafford CM, Kim JK, Hawker CJ, Russell TP. 2002 Asymmetric block copolymers with homopolymers: routes to multiple length scale nanostructures. *Adv. Mater.* **14**, 274–276. (doi:10.1002/1521-4095(20020219)14:4<274::AID-ADMA274>3.0.CO;2-M)
30. Jeong U, Ryu DY, Kim JK, Kim DH, Russell TP, Hawker CJ. 2003 Volume contractions induced by crosslinking: a novel route to nanoporous polymer films. *Adv. Mater.* **15**, 1247–1250. (doi:10.1002/adma.200304401)
31. Jeong U, Ryu DY, Kim JK, Kim DH, Wu X, Russell TP. 2003 Precise control of nanopore size in thin film using mixtures of asymmetric block copolymer and homopolymer. *Macromolecules* **36**, 10 126–10 129. (doi:10.1021/ma034976i)
32. Liu C-C, Nealey PF, Ting Y-H, Wendt AE. 2007 Pattern transfer using poly(styrene-block methyl methacrylate) copolymer films and reactive ion etching. *J. Vac. Sci. Technol. B* **25**, 1963–1968.
33. Asakawa K, Hiraoka T. 2002 Nanopatterning with microdomains of block copolymers using reactive-ion etching selectivity. *Jpn J. Appl. Phys.* **41**, 6112–6118. (doi:10.1143/JJAP.41.6112)

34. Zschech D, Kim DH, Milenin AP, Scholz R, Hillebrand R, Hawker CJ, Russell TP, Steinhart M, Gösele U. 2007 Ordered arrays of <100>-oriented silicon nanorods by CMOS-compatible block copolymer lithography. *Nano Lett.* **7**, 1516–1520.
35. Ting Y-H, Park S-M, Liu C-C, Liu X, Himpsel FJ, Nealey PF, Wendt AE. 2008 Plasma etch removal of poly(methyl methacrylate) in block copolymer lithography. *J. Vac. Sci. Technol. B* **26**, 1684. (doi:10.1116/1.2966433)
36. Farrell RA, Petkov N, Shaw MT, Djara V, Holmes JD, Morris MA. 2010 Monitoring PMMA elimination by reactive ion etching from a lamellar PS *b*-PMMA thin film by *ex situ* TEM methods. *Macromolecules* **43**, 8651–8655. (doi:10.1021/ma101827u)
37. Black CT, Guarini KW, Milkove KR, Baker SM, Russell TP, Tuominen MT. 2001 Integration of self-assembled diblock copolymers for semiconductor capacitor fabrication. *Appl. Phys. Lett.* **79**, 409–411. (doi:10.1063/1.1383805)
38. Thurn-Albrecht T *et al.* 2000 Ultrahigh-density nanowire arrays grown in self-assembled diblock copolymer templates. *Science* **290**, 2126–2129.
39. Guarini KW, Black CT, Milkove KR, Sandstrom RL. 2001 Nanoscale patterning using self-assembled polymers for semiconductor applications. *J. Vac. Sci. Technol. B* **19**, 2784. (doi:10.1116/1.1421551)
40. Liu K, Baker S, Tuominen M, Russell T, Schuller I. 2001 Tailoring exchange bias with magnetic nanostructures. *Phys. Rev. B* **63**, 060403. (doi:10.1103/PhysRevB.63.060403)
41. Choi D-G, Jeong J-R, Kwon KY, Jung H-T, Shin S-C, Yang S-M. 2004 Magnetic nanodot arrays patterned by selective ion etching using block copolymer templates. *Nanotechnology* **15**, 970–974. (doi:10.1088/0957-4484/15/8/018)
42. Jeong S-J, Xia G, Kim BH, Shin DO, Kwon S-H, Kang S-W, Kim SO. 2008 Universal block copolymer lithography for metals, semiconductors, ceramics, and polymers. *Adv. Mater.* **20**, 1898–1904. (doi:10.1002/adma.200702930)
43. Kim HC, Jia XQ, Stafford CM, Kim DH, McCarthy TJ, Tuominen M, Hawker CJ, Russell TP. 2001 A route to nanoscopic SiO_2 posts via block copolymer templates. *Adv. Mater.* **13**, 795–797. (doi:10.1002/1521-4095(200106)13:11<795::AID-ADMA795>3.0.CO;2-1)
44. Melde BJ, Burkett SL, Xu T, Goldbach JT, Russell TP, Hawker CJ. 2005 Silica nanostructures templated by oriented block copolymer thin films using pore-filling and selective-mineralization routes. *Chem. Mater.* **17**, 4743–4749. (doi:10.1021/cm051407b)
45. Zschech D *et al.* 2006 High-temperature resistant, ordered gold nanoparticle arrays. *Nanotechnology* **17**, 2122–2126.
46. Naito K, Hieda H, Sakurai M, Kamata Y, Asakawa K. 2002 2.5-inch disk patterned media prepared by an artificially assisted self-assembling method. *Magn. IEEE Trans.* **38**, 1949–1951. (doi:10.1109/TMAG.2002.802847)
47. Shin K, Leach KA, Goldbach JT, Kim DH, Jho JY, Tuominen M, Hawker CJ, Russell TP. 2002 A simple route to metal nanodots and nanoporous metal films. *Nano Lett.* **2**, 933–936. (doi:10.1021/nl0256560)
48. McGehee M, Misner M, Ryu D, Russell T. 2006 Fabrication of densely packed, well-ordered, high-aspect-ratio silicon nanopillars over large areas using block copolymer lithography. *Thin Solid Films* **513**, 289–294. (doi:10.1016/j.tsf.2006.01.064)
49. Xiao S, Yang X, Edwards EW, La Y-H, Nealey PF. 2005 Graphoepitaxy of cylinder-forming block copolymers for use as templates to pattern magnetic metal dot arrays. *Nanotechnology* **16**, S324. (doi:10.1088/0957-4484/16/7/003)
50. Peng Q, Tseng Y-C, Darling SB, Elam JW. 2010 Nanoscopic patterned materials with tunable dimensions via atomic layer deposition on block copolymers. *Adv. Mater.* **22**, 5129–5133. (doi:10.1002/adma.201002465)
51. Tseng Y-C, Peng Q, Ocola LE, Czaplewski DA, Elam JW, Darling SB. 2011 Etch properties of resists modified by sequential infiltration synthesis. *J. Vac. Sci. Technol. B* **29**, 06FG01–06FG014. (doi:10.1116/1.3640758)
52. Tseng Y-C, Peng Q, Ocola LE, Czaplewski DA, Elam JW, Darling SB. 2011 Enhanced polymeric lithography resists via sequential infiltration synthesis. *J. Mater. Chem.* **21**, 11 722–11 725. (doi:10.1039/C1JM12461G)
53. Peng Q, Tseng Y-C, Darling SB, Elam JW. 2011 A route to nanoscopic materials via sequential infiltration synthesis on block copolymer templates. *ACS Nano* **5**, 4600–4606. (doi:10.1021/nn2003234)

54. Tseng Y-C, Peng Q, Ocola LE, Elam JW, Darling SB. 2011 Enhanced block copolymer lithography using sequential infiltration synthesis. *J. Phys. Chem. C* **115**, 17 725–17 729. (doi:10.1021/jp205532e)
55. Kamcev J, Germack DS, Nykypanchuk D, Grubbs RB, Nam C-Y, Black CT. 2012 Chemically enhancing block copolymers for block-selective synthesis of self-assembled metal oxide nanostructures. *ACS Nano* **7**, 339–346. (doi:10.1021/nn304122b)
56. Kennemur JG, Hillmyer MA, Bates FS. 2012 Synthesis, thermodynamics, and dynamics of poly(4-tert-butylstyrene-b-methyl methacrylate). *Macromolecules* **45**, 7228–7236. (doi:10.1021/ma301047y)
57. Zhao Y, Sivaniah E, Hashimoto T. 2008 SAXS analysis of the order-disorder transition and the interaction parameter of polystyrene-*block*-poly(methyl methacrylate). *Macromolecules* **41**, 9948–9951. (doi:10.1021/ma8013004)
58. Cochran EW, Morse DC, Bates FS. 2003 Design of ABC triblock copolymers near the ODT with the random phase approximation. *Macromolecules* **36**, 782–792. (doi:10.1021/ma020651a)
59. Ren Y, Lodge TP, Hillmyer MA. 2000 Synthesis, characterization, and interaction strengths of difluorocarbene-modified polystyrene-polyisoprene block copolymers. *Macromolecules* **33**, 866–876. (doi:10.1021/ma9917085)
60. Dai KH, Kramer EJ. 1994 Determining the temperature-dependent Flory interaction parameter for strongly immiscible polymers from block copolymer segregation measurements. *Polymer* **35**, 157–161. (doi:10.1016/0032-3861(94)90065-5)
61. Zalusky AS, Olayo-Valles R, Wolf JH, Hillmyer MA. 2002 Ordered nanoporous polymers from polystyrene-polylactide block copolymers. *J. Am. Chem. Soc.* **124**, 12 761–12 773. (doi:10.1021/ja0278584)
62. Cushen JD, Bates CM, Rausch EL, Dean LM, Zhou SX, Willson CG, Ellison CJ. 2012 Thin film self-assembly of poly(trimethylsilylstyrene-b-D,L-lactide) with sub-10 nm domains. *Macromolecules* **45**, 8722–8728. (doi:10.1021/ma301238j)
63. Leiston-Belanger JM, Russell TP, Drockenmuller E, Hawker CJ. 2005 A thermal and manufacturable approach to stabilized diblock copolymer templates. *Macromolecules* **38**, 7676–7683. (doi:10.1021/ma0507847)
64. Keen I, Yu A, Cheng H-H, Jack KS, Nicholson TM, Whittaker AK, Blakey I. 2012 Control of the orientation of symmetric poly(styrene)-block-poly(D,L-lactide) block copolymers using statistical copolymers of dissimilar composition. *Langmuir* **28**, 15 876–15 888. (doi:10.1021/la304141m)
65. Vayer M, Hillmyer MA, Dirany M, Thevenin G, Erre R, Sinturel C. 2010 Perpendicular orientation of cylindrical domains upon solvent annealing thin films of polystyrene-*b*-polylactide. *Thin Solid Films* **518**, 3710–3715. (doi:10.1016/j.tsf.2009.10.015)
66. Olayo-Valles R, Lund MS, Leighton C, Hillmyer MA. 2004 Large area nanolithographic templates by selective etching of chemically stained block copolymer thin films. *J. Mater. Chem.* **14**, 2729–2731. (doi:10.1039/b408639b)
67. Baruth A, Rodwogin MD, Shankar A, Erickson MJ, Hillmyer MA, Leighton C. 2011 Non-lift-off block copolymer lithography of 25 nm magnetic nanodot arrays. *ACS Appl. Mater. Interfaces* **3**, 3472–3481. (doi:10.1021/am200693x)
68. Nguyen TH, Vayer M, Grosso D, Amenitsch H, Sinturel C. 2012 Using sol–gel replications to assess the porosity of block-copolymer derived thin films. *J. Phys. Chem. C* **116**, 5295–5302. (doi:10.1021/jp206926z)
69. Kim SH, Misner MJ, Xu T, Kimura M, Russell TP. 2004 Highly oriented and ordered arrays from block copolymers via solvent evaporation. *Adv. Mater.* **16**, 226–231. (doi:10.1002/adma.200304906)
70. Kim SH, Misner MJ, Russell TP. 2004 Solvent-induced ordering in thin film diblock copolymer/homopolymer mixtures. *Adv. Mater.* **16**, 2119–2123. (doi:10.1002/adma.200306577)
71. Bang J, Kim SH, Drockenmuller E, Misner MJ, Russell TP, Hawker CJ. 2006 Defect-free nanoporous thin films from ABC triblock copolymers. *J. Am. Chem. Soc.* **128**, 7622–7629. (doi:10.1021/ja0608141)
72. Zhang M, Yang L, Yurt S, Misner MJ, Chen JT, Coughlin EB, Venkataraman D, Russell TP. 2007 Highly ordered nanoporous thin films from cleavable polystyrene-*block*-poly(ethylene oxide). *Adv. Mater.* **19**, 1571–1576. (doi:10.1002/adma.200602461)

73. Zhao H, Gu W, Sterner E, Russell TP, Coughlin EB, Theato P. 2011 Highly ordered nanoporous thin films from photocleavable block copolymers. *Macromolecules* **44**, 6433–6440. (doi:10.1021/ma201416b)
74. Gu X, Liu Z, Gunkel I, Chourou ST, Hong SW, Olynick DL, Russell TP. 2012 High aspect ratio sub-15 nm silicon trenches from block copolymer templates. *Adv. Mater.* **24**, 5688–5694. (doi:10.1002/adma.201202361)
75. Mao H, Hillmyer MA. 2005 Nanoporous polystyrene by chemical etching of poly(ethylene oxide) from ordered block copolymers. *Macromolecules* **38**, 4038–4039. (doi:10.1021/ma050008z)
76. Kim DH, Kim SH, Lavery K, Russell TP. 2004 Inorganic nanodots from thin films of block copolymers. *Nano Lett.* **4**, 1841–1844. (doi:10.1021/nl049063w)
77. Xu J, Hong SW, Gu W, Lee KY, Kuo DS, Xiao S, Russell TP. 2011 Fabrication of silicon oxide nanodots with an areal density beyond 1 teradots inch-2. *Adv. Mater.* **23**, 5755–5761. (doi:10.1002/adma.201102964)
78. Kim H-C, Cheng J, Park O-H, Park S-M, Ruiz R, Black CT, Pitera J, Rettner C, Flickner M. 2008 Rapid directed self-assembly of lamellar microdomains from a block copolymer containing hybrid. *Adv. Lithogr.* **6925**, 692129. (doi:10.1117/12.772684)
79. Kim H-C, Rettner CT, Sundström L. 2008 The fabrication of 20 nm half-pitch gratings by corrugation-directed self-assembly. *Nanotechnology* **19**, 235301. (doi:10.1088/0957-4484/19/23/235301)
80. Freer EM, Krupp LE, Hinsberg WD, Rice PM, Hedrick JL, Cha JN, Miller RD, Kim H-C. 2005 Oriented mesoporous organosilicate thin films. *Nano Lett.* **5**, 2014–2018. (doi:10.1021/nl051517 h)
81. Park S, Wang J-Y, Kim B, Xu J, Russell TP. 2008 A simple route to highly oriented and ordered nanoporous block copolymer templates. *ACS Nano* **2**, 766–772. (doi:10.1021/nn7004415)
82. Sundström L, Krupp L, Delenia E, Rettner C, Sanchez M, Hart MW, Kim H-C, Zhang Y. 2006 Patterning ~20 nm half-pitch lines on silicon using a self-assembled organosilicate etch mask. *Appl. Phys. Lett.* **88**, 243107. (doi:10.1063/1.2205178)
83. Park S-M, Park O-H, Cheng JY, Rettner CT, Kim H-C. 2008 Patterning sub-10 nm line patterns from a block copolymer hybrid. *Nanotechnology* **19**, 455304. (doi:10.1088/0957-4484/19/45/455304)
84. Cheng JY, Pitera J, Park O-H, Flickner M, Ruiz R, Black CT, Kim H-C. 2007 Rapid directed self assembly of lamellar microdomains from a block copolymer containing hybrid. *Appl. Phys. Lett.* **91**, 143106. (doi:10.1063/1.2791003)
85. Spatz JP, Herzog T, Mößmer S, Ziemann P, Möller M. 1999 Micellar inorganic-polymer hybrid systems—a tool for nanolithography. *Adv. Mater.* **11**, 149–153. (doi:10.1002/(SICI)1521-4095(199902)11:2<149::AID-ADMA149>3.0.CO;2-W)
86. Spatz J, Mößmer S, Hartmann C, Möller M. 2000 Ordered deposition of inorganic clusters from micellar block copolymer films. *Langmuir* **16**, 407–415. (doi:10.1021/la990070n)
87. Chai J, Wang D, Fan XN, Buriak JM. 2007 Assembly of aligned linear metallic patterns on silicon. *Nat. Nanotechnol.* **2**, 500–506. (doi:10.1038/nnano.2007.227)
88. Chai J, Buriak JM. 2008 Using cylindrical domains of block copolymers to self-assemble and align metallic nanowires. *ACS Nano* **2**, 489–501. (doi:10.1021/nn700341s)
89. Mizuno H, Buriak JM. 2009 Nanoscale patterning of organic monolayers by catalytic stamp lithography: scope and limitations. *ACS Appl. Mater. Interfaces* **1**, 2711–2720. (doi:10.1021/am900602m)
90. Park S, Wang JY, Kim B, Chen W, Russell TP. 2007 Solvent-induced transition from micelles in solution to cylindrical microdomains in diblock copolymer thin films. *Macromolecules* **40**, 9059–9063. (doi:10.1021/ma071321z)
91. Park S, Kim B, Wang JY, Russell TP. 2008 Fabrication of highly ordered silicon oxide dots and stripes from block copolymer thin films. *Adv. Mater.* **20**, 681–685. (doi:10.1002/adma.200701997)
92. Park S, Kim B, Yavuzcetin O, Tuominen MT, Russell TP. 2008 Ordering of PS-*b*-P4VP on patterned silicon surfaces. *ACS Nano* **2**, 1363–1370. (doi:10.1021/nn800073f)
93. Park S, Kim B, Xu J, Hofmann T, Ocko BM, Russell TP. 2009 Lateral ordering of cylindrical microdomains under solvent vapor. *Macromolecules* **42**, 1278–1284. (doi:10.1021/ma802480 s)
94. Park S, Yavuzcetin O, Kim B, Tuominen MT, Russell TP. 2009 A simple top-down/bottom-up approach to sectored, ordered arrays of nanoscopic elements using block copolymers. *Small* **5**, 1064–1069. (doi:10.1002/smll.200801573)

95. Park S, Kim B, Cirpan A, Russell TP. 2009 Preparation of metallic line patterns from functional block copolymers. *Small* **5**, 1343–1348. (doi:10.1002/smll.200801409)
96. Gu X, Dorsey P, Russell TP. 2012 High density and large area arrays of silicon oxide pillars with tunable domain size for mask etch applications. *Adv. Mater.* **24**, 5505–5511. (doi:10.1002/adma.201201278)
97. Bang BM, Kim H, Lee J-P, Cho J, Park S. 2011 Mass production of uniform-sized nanoporous silicon nanowire anodes via block copolymer lithography. *Energy Environ. Sci.* **4**, 3395–3399. (doi:10.1039/C1EE01898A)
98. Lee J-P, Bang BM, Choi S, Kim T, Park S. 2011 Patterning of various silicon structures via polymer lithography and catalytic chemical etching. *Nanotechnology* **22**, 275305. (doi:10.1088/0957-4484/22/27/275305)
99. Qiao Y, Wang D, Buriak JM. 2007 Block copolymer templated etching on silicon. *Nano Lett.* **7**, 464–469. (doi:10.1021/nl0627801)
100. Zhang X, Harris KD, Wu NLY, Murphy JN, Buriak JM. 2010 Fast assembly of ordered block copolymer nanostructures through microwave annealing. *ACS Nano* **4**, 7021–7029. (doi:10.1021/nn102387c)
101. Zhang X, Murphy JN, Wu NLY, Harris KD, Buriak JM. 2011 Rapid assembly of nanolines with precisely controlled spacing from binary blends of block copolymers. *Macromolecules* **44**, 9752–9757. (doi:10.1021/ma202064t)
102. Wu NLY, Zhang X, Murphy JN, Chai J, Harris KD, Buriak JM. 2012 Density doubling of block copolymer templated features. *Nano Lett.* **12**, 264–268. (doi:10.1021/nl203488a)
103. Du P *et al.* 2004 Additive-driven phase-selective chemistry in block copolymer thin films: the convergence of top–down and bottom–up approaches. *Adv. Mater.* **16**, 953–957. (doi:10.1002/adma.200306189)
104. Li M, Douki K, Goto K, Li X, Coenjarts C, Smilgies D-M, Ober CK. 2004 Spatially controlled fabrication of nanoporous block copolymers. *Chem. Mater.* **16**, 3800–3808. (doi:10.1021/cm0493445)
105. Bosworth JK, Paik MY, Ruiz R, Schwartz EL, Huang JQ, Ko AW, Smilgies D-M, Black CT, Ober CK. 2008 Control of self-assembly of lithographically patternable block copolymer films. *ACS Nano* **2**, 1396–1402. (doi:10.1021/nn8001505)
106. Bosworth JK, Black CT, Ober CK. 2009 Selective area control of self-assembled pattern architecture using a lithographically patternable block copolymer. *ACS Nano* **3**, 1761–1766. (doi:10.1021/nn900343u)
107. Zhang X, Sushkov AB, Metting CJ, Fackler S, Drew HD, Briber RM. 2012 Silicon patterning using self-assembled PS-*b*-PAA diblock copolymer masks for black silicon fabrication via plasma etching. *Plasma Process. Polym.* **9**, 968–974. (doi:10.1002/ppap.201100198)
108. Tang CB, Bang J, Stein GE, Fredrickson GH, Hawker CJ, Kramer EJ, Sprung M, Wang J. 2008 Square packing and structural arrangement of ABC triblock copolymer spheres in thin films. *Macromolecules* **41**, 4328–4339. (doi:10.1021/ma800207n)
109. Xiao SG, Yang XM, Park SJ, Weller D, Russell TP. 2009 A novel approach to addressable 4 teradot/in.(2) patterned media. *Adv. Mater.* **21**, 2516–2519. (doi:10.1002/adma.200802087)
110. Son JG, Gotrik KW, Ross CA. 2012 High-aspect-ratio perpendicular orientation of PS-b-PDMS thin films under solvent annealing. *ACS Macro Lett.* **1**, 1279–1284. (doi:10.1021/mz300475 g)
111. Bates CM, Seshimo T, Maher MJ, Durand WJ, Cushen JD, Dean LM, Blachut G, Ellison CJ, Willson CG. 2012 Polarity-switching top coats enable orientation of sub–10-nm block copolymer domains. *Science* **338**, 775–779. (doi:10.1126/science.1226046)
112. Jung YS, Ross CA. 2007 Orientation-controlled self-assembled nanolithography using a polystyrene-polydimethylsiloxane block copolymer. *Nano Lett.* **7**, 2046–2050. (doi:10.1021/nl070924 l)
113. Jung YS, Ross CA. 2009 Well-ordered thin-film nanopore arrays formed using a block-copolymer template. *Small* **5**, 1654–1659. (doi:10.1002/smll.200900053)
114. Jung YS, Jung W, Ross CA. 2008 Nanofabricated concentric ring structures by templated self-assembly of a diblock copolymer. *Nano Lett.* **8**, 2975–2981. (doi:10.1021/nl802011w)
115. Jung YS, Lee JH, Lee JY, Ross CA. 2010 Fabrication of diverse metallic nanowire arrays based on block copolymer self-assembly. *Nano Lett.* **10**, 3722–3726. (doi:10.1021/nl1023518)
116. Jung YS, Chang JB, Verploegen E, Berggren KK, Ross CA. 2010 A path to ultranarrow patterns using self-assembled lithography. *Nano Lett.* **10**, 1000–1005. (doi:10.1021/nl904141r)

117. Rodwogin MD, Baruth A, Jackson EA, Leighton C, Hillmyer MA. 2012 Nanoscale rings from silicon-containing triblock terpolymers. *ACS Appl. Mater. Interfaces* **4**, 3550–3557. (doi:10.1021/am300603x)
118. Lammertink R, Hempenius M, Chan V, Thomas E, Vancso G. 2001 Poly(ferrocenyldimethylsilanes) for reactive ion etch barrier applications. *Chem. Mater.* **13**, 429–434. (doi:10.1021/cm001052q)
119. Lammertink R, Hempenius MA, Thomas EL, Vancso GJ. 1999 Periodic organic-organometallic microdomain structures in poly(styrene-*block*-ferrocenyldimethylsilane) copolymers and blends with corresponding homopolymers. *J. Polym. Sci. B-Polym. Phys.* **37**, 1009–1021. (doi:10.1002/(SICI)1099-0488(19990515)37:10<1009::AID-POLB6>3.0.CO;2-W)
120. Li W, Sheller N, Foster MD, Balaishis D, Manners I, Annís B, Lin JS. 2000 Morphology and ordering behavior of a poly(styrene)-*b*-poly(ferrocenyldimethylsilane) diblock copolymer. *Polymer* **41**, 719–724. (doi:10.1016/S0032-3861(99)00176-7)
121. Lammertink R, Hempenius M, van den Enk J, Chan V, Thomas E, Vancso G. 2000 Nanostructured thin films of organic-organometallic block copolymers: one-step lithography with poly(ferrocenylsilanes) by reactive ion etching. *Adv. Mater.* **12**, 98–103. (doi:10.1002/(SICI)1521-4095(200001)12:2<98::AID-ADMA98>3.0.CO;2-5)
122. Temple K, Kulbaba K, Power-Billard KN, Manners I, Leach KA, Xu T, Russell TP, Hawker CJ. 2003 Spontaneous vertical ordering and pyrolytic formation of nanoscopic ceramic patterns from poly(styrene-*b*-ferrocenylsilane). *Adv. Mater.* **15**, 297–300. (doi:10.1002/adma.200390071)
123. Rider DA *et al.* 2008 Nanostructured magnetic thin films from organometallic block copolymers: pyrolysis of self-assembled polystyrene-*block*-poly(ferrocenylethylmethylsilane). *ACS Nano* **2**, 263–270. (doi:10.1021/nn7002629)
124. Ramanathan M, Nettleton E, Darling SB. 2009 Simple orientational control over cylindrical organic–inorganic block copolymer domains for etch mask applications. *Thin Solid Films* **517**, 4474–4478. (doi:10.1016/j.tsf.2009.02.078)
125. Ramanathan M, Darling SB. 2009 Thickness dependent hierarchical meso/nano scale morphologies of a metal-containing block copolymer thin film induced by hybrid annealing and their pattern transfer abilities. *Soft Matter* **5**, 4665. (doi:10.1039/b902114k)
126. Cheng J, Ross C, Chan V, Thomas E, Lammertink R, Vancso G. 2001 Formation of a cobalt magnetic dot array via block copolymer lithography. *Adv. Mater.* **13**, 1174–1178. (doi:10.1002/1521-4095(200108)13:15<1174::AID-ADMA1174>3.0.CO;2-Q)
127. Chang S-W, Chuang VP, Boles ST, Ross CA, Thompson CV. 2009 Densely packed arrays of ultra-high-aspect-ratio silicon nanowires fabricated using block-copolymer lithography and metal-assisted etching. *Adv. Funct. Mater.* **19**, 2495–2500. (doi:10.1002/adfm.200900181)
128. Bates FS, Fredrickson GH. 1999 Block copolymers-designer soft materials. *Phys. Today* **52**, 32–38. (doi:10.1063/1.882522)
129. Guo S, Rzayev J, Bailey TS, Zalusky AS, Olayo-Valles R, Hillmyer MA. 2006 Nanopore and nanobushing arrays from ABC triblock thin films containing two etchable blocks. *Chem. Mater.* **18**, 1719–1721. (doi:10.1021/cm052694 m)
130. Chuang VP, Ross CA, Gwyther J, Manners I. 2009 Self-assembled nanoscale ring arrays from a polystyrene-b-polyferrocenylsilane-b-poly(2-vinylpyridine)triblock terpolymer thin film. *Adv. Mater.* **21**, 3789–3793. (doi:10.1002/adma.200900756)
131. Chuang VP, Gwyther J, Mickiewicz RA, Manners I, Ross CA. 2009 Templated self-assembly of square symmetry arrays from an ABC triblock terpolymer. *Nano Lett.* **9**, 4364–4369. (doi:10.1021/nl902646e)
132. Son JG, Gwyther J, Chang J-B, Berggren KK, Manners I, Ross CA. 2012 Highly ordered square arrays from a templated ABC triblock terpolymer. *Nano Lett.* **11**, 2849–2855. (doi:10.1021/nl201262f)
133. Choi HK, Gwyther J, Manners I, Ross CA. 2012 Square arrays of holes and dots patterned from a linear ABC triblock terpolymer. *ACS Nano* **6**, 8342–8348. (doi:10.1021/nn303085k)
134. Hirai T *et al.* 2009 One-step direct-patterning template utilizing self-assembly of POSS-containing block copolymers. *Adv. Mater.* **21**, 4334–4338. (doi:10.1002/adma.200900518)
135. Tada Y *et al.* 2012 Directed self-assembly of POSS containing block copolymer on lithographically defined chemical template with morphology control by solvent vapor. *Macromolecular* **45**, 292–304. (doi:10.1021/ma201822a)

136. Lin Y-C, Kuo S-W. 2012 Hierarchical self-assembly structures of POSS-containing polypeptide block copolymers synthesized using a combination of ATRP, ROP and click chemistry. *Polym. Chem.* **3**, 882. (doi:10.1039/c2py00574c)
137. Otsuka I, Isono T, Rochas C, Halila S, Fort S, Satoh T, Kakuchi T, Borsali R. 2012 10 nm scale cylinder–cubic phase transition induced by caramelization in sugar-based block copolymers. *ACS Macro Lett.* **1**, 1379–1382. (doi:10.1021/mz300543u)
138. Cushen JD *et al.* 2012 Oligosaccharide/silicon-containing block copolymers with 5 nm features for lithographic applications. *ACS Nano* **6**, 3424–3433. (doi:10.1021/nn300459r)
139. Ku SJ, Kim SM, Bak CH, Kim J-B. 2011 Nanoporous hard etch masks using silicon-containing block copolymer thin films. *Polymer* **52**, 86–90. (doi:10.1016/j.polymer.2010.11.012)
140. Jeong JW, Park WI, Kim M-J, Ross CA, Jung YS. 2011 Highly tunable self-assembled nanostructures from a poly(2-vinylpyridine-b-dimethylsiloxane) block copolymer. *Nano Lett.* **11**, 4095–4101. (doi:10.1021/nl2016224)
141. Lee J-Y, Shiao M-C, Tzeng F-Y, Chang C-H, Tsai C-K, Tsai J-C, Lo K-H, Lin S-C, Ho R-M. 2012 Syndiotactic polyallyltrimethylsilane-based stereoregular diblock copolymers: syntheses and self-assembled nanostructures. *Macromolecules* **45**, 2720–2730. (doi:10.1021/ma300034f)
142. Bates CM, Pantoja MAB, Strahan JR, Dean LM, Mueller BK, Ellison CJ, Nealey PF, Willson CG. 2012 Synthesis and thin-film orientation of poly(styrene-block-trimethylsilylisoprene). *J. Polym. Sci. Pol. Chem.* **51**, 290–297. (doi:10.1002/pola.26375)
143. Rodwogin MD, Spanjers CS, Leighton C, Hillmyer MA. 2010 Polylactide-poly(dimethylsiloxane)-polylactide triblock copolymers as multifunctional materials for nanolithographic applications. *ACS Nano* **4**, 725–732. (doi:10.1021/nn901190a)
144. Darling SB. 2007 Directing the self-assembly of block copolymers. *Prog. Polym. Sci.* **32**, 1152–1204. (doi:10.1016/j.progpolymsci.2007.05.004)
145. Marencic AP, Register RA. 2010 Controlling order in block copolymer thin films for nanopatterning applications. *Annu. Rev. Chem. Biomol. Eng.* **1**, 277–297. (doi:10.1146/annurev-chembioeng-073009-101007)
146. Ryu DY, Shin K, Drockenmuller E, Hawker CJ, Russell TP. 2005 A generalized approach to the modification of solid surfaces. *Science* **308**, 236–239. (doi:10.1126/science.1106604)
147. Segalman RA, Yokoyama H, Kramer EJ. 2001 Graphoepitaxy of spherical domain block copolymer films. *Adv. Mater.* **13**, 1152–1155. (doi:10.1002/1521-4095(200108)13:15<1152::AID-ADMA1152>3.0.CO;2-5)
148. Hong SW, Gu X, Huh J, Xiao S, Russell TP. 2011 Circular nanopatterns over large areas from the self-assembly of block copolymers guided by shallow trenches. *ACS Nano* **5**, 2855–2860. (doi:10.1021/nn103401w)
149. Hong SW, Huh J, Gu X, Lee DH, Jo WH, Park S, Xu T, Russell TP. 2012 Unidirectionally aligned line patterns driven by entropic effects on faceted surfaces. *Proc. Natl Acad. Sci. USA* **109**, 1402–1406. (doi:10.1073/pnas.1115803109)
150. Cheng JY, Mayes AM, Ross CA. 2004 Nanostructure engineering by templated self-assembly of block copolymers. *Nat. Mater.* **3**, 823–828. (doi:10.1038/nmat1211)
151. Bita I, Yang JKW, Jung YS, Ross CA, Thomas EL, Berggren KK. 2008 Graphoepitaxy of self-assembled block copolymers on two-dimensional periodic patterned templates. *Science* **321**, 939–943. (doi:10.1126/science.1159352)
152. Yang JKW, Jung YS, Chang J-B, Mickiewicz RA, Alexander-Katz A, Ross CA, Berggren KK. 2010 Complex self-assembled patterns using sparse commensurate templates with locally varying motifs. *Nat. Nanotechnol.* **5**, 256–260. (doi:10.1038/nnano.2010.30)
153. Tavakkoli KGA, Gotrik KW, Hannon AF, Alexander-Katz A, Ross CA, Berggren KK. 2012 Templating three-dimensional self-assembled structures in bilayer block copolymer films. *Science* **336**, 1294–1298. (doi:10.1126/science.1218437)
154. Rockford L, Liu Y, Mansky P, Russell T, Yoon M, Mochrie S. 1999 Polymers on nanoperiodic, heterogeneous surfaces. *Phys. Rev. Lett.* **82**, 2602–2605. (doi:10.1103/PhysRevLett.82.2602)
155. Stoykovich MP, Muller M, Kim SO, Solak HH, Edwards EW, de Pablo JJ, Nealey PF. 2005 Directed assembly of block copolymer blends into nonregular device-oriented structures. *Science* **308**, 1442–1446. (doi:10.1126/science.1111041)
156. Kim SO, Solak HH, Stoykovich MP, Ferrier NJ, de Pablo JJ, Nealey PF. 2003 Epitaxial self-assembly of block copolymers on lithographically defined nanopatterned substrates. *Nature* **424**, 411–414. (doi:10.1038/nature01775)

157. Ruiz R, Kang H, Detcheverry FA, Dobisz E, Kercher DS, Albrecht TR, de Pablo JJ, Nealey PF. 2008 Density multiplication and improved lithography by directed block copolymer assembly. *Science* **321**, 936–939. (doi:10.1126/science.1157626)
158. Ross CA, Cheng JY. 2008 Patterned magnetic media made by self-assembled block-copolymer lithography. *MRS Bull.* **33**, 838–845. (doi:10.1557/mrs2008.179)
159. Päivänranta B *et al.* 2011 Nanofabrication of broad-band antireflective surfaces using self-assembly of block copolymers. *ACS Nano* **5**, 1860–1864. (doi:10.1021/nn103361d)
160. Bai J, Zhong X, Jiang S, Huang Y, Duan X. 2010 Graphene nanomesh. *Nat. Nanotechnol.* **5**, 190–194. (doi:10.1038/nnano.2010.8)
161. Jung YS, Jung W, Tuller HL, Ross CA. 2008 Nanowire conductive polymer gas sensor patterned using self-assembled block copolymer lithography. *Nano Lett.* **8**, 3776–3780. (doi:10.1021/nl802099k)
162. Lu J, Chamberlin D, Rider DA, Liu M, Manners I, Russell TP. 2006 Using a ferrocenylsilane-based block copolymer as a template to produce nanotextured Ag surfaces: uniformly enhanced surface enhanced Raman scattering active substrates. *Nanotechnology* **17**, 5792–5797. (doi:10.1088/0957-4484/17/23/014)
163. Bates FS, Hillmyer MA, Lodge TP, Bates CM, Delaney KT, Fredrickson GH. 2012 Multiblock polymers: panacea or pandora's box? *Science* **336**, 434–440. (doi:10.1126/science.1215368)